Perspective

Challenges and opportunities in 2D heterostructures for electronic and optoelectronic devices

Suman Kumar Chakraborty,[1] Baisali Kundu,[1] Biswajeet Nayak,[1] Saroj Prasad Dash,[2,*] and Prasana Kumar Sahoo[1,*]

SUMMARY

Two-dimensional (2D) materials such as graphene, transition metal dichalcogenides (TMDs), and their heterojunctions are prospective materials for future electronics, optoelectronics, and quantum technologies. Assembling different 2D layers offers unique ways to control optical, electrical, thermal, magnetic, and topological phenomena. Controlled fabrications of electronic grade 2D heterojunctions are of paramount importance. Here, we enlist novel and scalable strategies to fabricate 2D vertical and lateral heterojunctions, consisting of semiconductors, metals, and/or semimetals. Critical issues that need to be addressed are the device-to-device variations, reliability, stability, and performances of 2D heterostructures in electronic and optoelectronic applications. Also, stacking order-dependent formation of moiré excitons in 2D heterostructures are emerging with exotic physics and new opportunities. Furthermore, the realization of 2D heterojunction-based novel devices, including excitonic and valleytronic transistors, demands more extensive research efforts for real-world applications. We also outline emergent phenomena in 2D heterojunctions central to nanoelectronics, optoelectronics, spintronics, and energy applications.

INTRODUCTION

Silicon-based field-effect transistors (FETs) are the backbone of our modern semiconducting technology. Through relentless miniaturization of FETs over the past five decades, followed by Moore's law to sustain continuous improvement in performance for the fabrication of more powerful, efficient, and advanced electronic components with better speed and computing power, the size of the FETs has down to the nano-scale. Subsequently, further enhancement in performance is not possible via downscaling, limited by size, inadequate carrier mobility, short channel effects, atomic-scale interactions, heat generation, and energy consumption at atomic scale thickness. To overcome the limitations of further miniaturization, tremendous research efforts have been opted worldwide to find a new strategy. The most viable approach that could successfully encounter the challenges faced by silicon electronics is the replacement of silicon with a novel class of materials such as 'two-dimensional (2D) materials', 'Quantum materials' or 'van der Waals (vdW) materials' having an atomic level thickness (Liu et al., 2021). The journey of 2D materials started in 2004 with the successful manual isolation of graphene by mechanical exfoliation technique (Novoselov et al., 2004), and for the past 17 years, graphene and graphene-like 2D materials [e.g. transition metal dichalcogenides (TMDs), hexagonal boron nitride (h-BN), and black phosphorus (BP)] are investigated extensively because of their exceptional electro-optical functionalities, which are not accessible in their bulk counterparts. Astonishingly, it has been recently predicted that 1825 mechanically exfoliate vdW materials can be thinned down to monolayer (Mounet et al., 2018), and thus many more exciting functionalities are pending for the near future. The library of ultrathin two-dimensional layered materials (2DLMs) is showcased with metallic, semi-metallic, semiconducting, insulating, superconducting, topological insulator electronic subgroups (Ma et al., 2018). Unlike graphene with zero bandgaps at Dirac points, semiconducting 2D TMDs in the MX_2 stoichiometry [M = (W, Mo) and X = (S, SE, Te)] are promising candidates for impending quantum optoelectronics, electronics, valleytronics, photonics, sensors, energy harvesting, and flexible devices applications, owing to direct bandgap ranging from visible to infrared region (Mak and Shan, 2016), strong excitonic effect (Chernikov et al., 2014), strong light-matter interaction (Britnell et al., 2013; Mak et al., 2010), spin-valley coupling (Xiao et al., 2012), operative carrier mobility (Radisavljevic et al., 2011) and valley polarization (Zeng et al., 2012) in monolayer limit. In addition, flexibility in tuning

[1]Materials Science Centre, Quantum Materials and Device Research Laboratory, Indian Institute of Technology Kharagpur, Kharagpur, West Bengal, India

[2]Department of Microtechnology and Nanoscience, Quantum Device Physics Laboratory, Chalmers University of Technology, Göteborg, Sweden

*Correspondence:
saroj.dash@chalmers.se
(S.P.D.),
prasana@matsc.iitkgp.ac.in
(P.K.S.)
https://doi.org/10.1016/j.isci.2022.103942

electronic bandstructure via layer number, alloying, and doping strategies arouse paramount interest in TMDs than other 2D materials (Chaves et al., 2020; Nugera et al., 2021). Intriguing functionalities, endowed by 2D nature, open up new opportunities to fabricate efficient, ultra-high-speed electronic and optoelectronic quantum devices. However, the pathway of 2D materials and their heterostructures (HSs) toward a high-performance flexible and efficient technology is still in its nascent stage and poses many challenges from interface quality to stability and reliability. Hence, it is crucial to uplift recent strategies for unique device designs and subsequent statistical performance analysis. Co-integration of monolayers from different 2DLMs in vertical and lateral geometry gives unprecedented access to new functionalities and offers unique ways to manipulate profound optical and electrical properties with better chemical and environmental stability, which can be helpful to design on-demand electronic, optoelectronic devices and harnessing excitonic states. These novel materials' viability is not only limited to electronics, optoelectronics, and the fields mentioned above; they are equally potential to use as memtransistors, biosensors, and to develop 'Internet of Things' (Briggs et al., 2019; Sangwan et al., 2018).

Materials preparation is the first step to commercialize 2D materials and HS-based applications from laboratory to industrial scale. To that end, vertical integration of mechanically isolated monolayers into vdW HS via layer by layer transfer process does not pose any limitation on lattice matching, as individual layers are coupled to each other through weak vdW interaction. This feature of vdW HS offers unparalleled freedom to combine different 2DLMs with exploring various exotic functionalities, which are tunable through constituent layers stacking order, mutual rotation, and external fields. However, interfacial contamination and lack of scalability issues in the 2D transfer process limit their intended performance and use on a large scale. Consequently, direct epitaxial growth is the only way to achieve clean interfaces and scalable vertical heterostructure (VHS). Whereas direct epitaxial growth of lateral heterostructure (LHS) in the form of the 2D plane is only possible via direct growth to realize lateral integration, dictated by lattice structure matching, which offers exciting functionalities holding individual monolayers-properties at ultimate thickness including intrinsic p-n diode-like and photovoltaic response (Sahoo et al., 2018, 2019), persistent photoconductivity (Berweger et al., 2020). In this account, chemical vapor deposition (CVD) has emerged as a promising method to fabricate wafer-scale samples because of its simplicity, cost-effectiveness, scalability, and high-quality sample output. However, it poses significant challenges that need immediate attention to push 2D electronics and optoelectronics to a new height. Among the developed CVD strategies, the water-assisted one-pot method, pioneered by Sahoo et al., is the most simple, robust, scalable, and commercially viable approach so far (Sahoo et al., 2018). In addition, direct vertical heterointegration of different 2D TMDs, graphene, and boron nitride are the need of the hour for device scalability. VHSs with little or different twist angles are emerging for fundamental research and novel applications. Excitonic devices, moiré superlattice, and moiré excitons in the 2D domain show appealing research attention for their novel functionalities that unlock future quantum technology.

In this perspective, we have started the discussion with an outlined overview of mechanical transfer techniques to draw attention to the stringent requirement of developing CVD strategies for the direct fabrication of 2D heterostructures. Different CVD strategies carried out to synthesize scalably and high-quality HSs are summarized with advantages and shortcomings over each other, followed by an overview of possible growth mechanisms for vertical and lateral integration and future targets for CVD toward harnessing recently observed fascinating 2D physics into real-world applications. Different excitons and emergent quantum phases in twisted systems, which bring the outstanding possibility for next-generation technology, are discussed with upcoming opportunities. Potential applications of 2D HSs are also outlined with their challenges and unprecedented expectations from them. Especially, FETs and tunneling field-effect transistors (TFET) are highlighted for electronic and low-power uses. Finally, we discussed with possible outlook in this emerging field that can pose a 3D to the 2D technological paradigm shift in the forthcoming years to revolutionize our lifestyle. Overall, we hope to convey CVD as an unrivaled approach to mature the urgently growing demand for 2D electronics, optoelectronics, and next-generation technology from research scale to commercialization via enabling device fabrication.

FABRICATION OF HETEROSTRUCTURES

Monolayer or bilayer TMD HSs are ideal candidates for the efficient extraction of the charge carriers with diverse functionality for electronics and optoelectronics. However, interface quality plays a divisive role in the overall device characteristic, reliability, and performance in the vertical or lateral configuration. A wide variation in the performance even for a specific TMD and its heterostructure has been found because of the

variation in the material qualities from different growth processes and sensitivity to the various experimental environments. In addition, local defects, source impurities, surface roughness, gas adsorbates, etc., can also significantly affect carrier generation and transportation.

Mechanical transfer

To date, the mechanical transfer method is the most lucid, straightforward, and popular tool that we have to fabricate different 2D vdW HSs. It follows a simple procedure in which mechanically exfoliated one 2D material's monolayer is transferred on top of another or others in vertical order (Zomer et al., 2011, 2014). An optical microscope and micromanipulator are used to locate and precisely align the 2D flakes properly to carry out the layer-by-layer stacking task in conjunction with manual operation. In the company of intrinsic functionalities, substrate plays a decisive role in the performance of 2D monolayers and heterostructures-based devices. Compared to a single layer, bilayer HSs show less susceptibility to the substrate. After discovering graphene, SiO_2/Si was widely employed as a substrate for graphene electronics. Still, their performance metrics were far inferior to the expectation because of the detrimental role of unavoidable surface roughness, surface pinning, and dangling bonds in overall device performance. To overcome such issues, either a free-standing flake can be used or need an atomically flat dielectric such as 2D hexagonal boron nitride (hBN). Though the choice of the substrate provides substantial performance improvement (Du et al., 2008), the progress is limited by the complex device design, scalability, and long-term environmental stability. 2D h-BN has emerged as a good insulator for substrate, gate dielectrics, and tunnel barriers for its ultra-thinness, large bandgap, atomically smooth, and dangling bond-free surface (Dankert et al., 2017; Dean et al., 2010; Kamalakar et al., 2016). However, its large-scale fabrication with controlled layer number and cost is a bottleneck to large-scale use. Several approaches have been routinely employed to execute the 2D transfer process, like polymethyl-methacrylate and water-soluble layer assisted method (Dean et al., 2010), wedging method (Calado et al., 2012), and Elvacite method (Zomer et al., 2011), which relies on sacrificial polymeric layers and wet chemistry, water intercalation followed by cleaning the residual using acetone. Indeed, the fabricated 2D assembles using the above wet-transfer techniques are prone to contamination due to chemical and polymeric residues and capillary forces. On the other hand, dry transfer methods are an appealing alternative. Polymer-free deterministic stacking via the all-dry viscoelastic stamping technique (Castellanos-Gomez et al., 2014) has also been employed to fabricate high-quality 2D HSs. The above top-down strategies are limited to a few micron flake sizes because of the fragmentation of the large area patches as a consequence of the comparatively low adhesion of silicon wafers to the 2D materials. Taking advantage of the strong affinity of 2D materials to the metal, researchers recently exfoliated monolayer flakes of millimeter-scale with high yield and stacked them to get heterobilayer of few millimeter sizes via gold assistance exfoliation and transfer (Huang et al., 2020). Although these methods are feasible to study fundamental sciences but limited by many shortcomings that include; 1) scalability for mass production of devices, 2) limited to vertical stacking geometry, whereas atomically in-plane stitched LHS cannot be realized, 3) low-throughput and time-consuming, 4) cumbersome process, and 5) lack of control on the proper positional and angular alignment of 2D flakes. In these contexts, direct and scalable fabrication of HSs via CVD or metal-organic chemical vapor deposition (MOCVD) can serve the ultimate purposes, which are the stringent need of the hour.

CVD strategy for 2D heterostructures

CVD is a routinely used materials processing technique in the semiconducting industry that relies on the chemical reactions between the gas phase adsorbates of the solid precursors on the substrate surface at an elevated temperature that promotes heterogeneous nucleation. This process is advantageous over other techniques to control crystallinity, domain size, and high electronic quality with high yield. With the potential for industrial applications to complement 3D semiconducting technology, it is also promising for the next-generation flexible and transparent 2D technology. Different CVD strategies have been developed to synthesize 2D materials and HSs in the past few years. Several efforts are ongoing worldwide to develop electronic grade 2D materials and their heterostructures with excellent structural, optical, and electronic qualities and controllability, which are still posing severe challenges in their pathway to commercialization. A critical overview regarding the roadmap toward commercialization (Figure 1) and current state-of-the-art technologies for the CVD growth of various TMDs based HSs is addressed in the following sections. A comprehensive future target is put forward toward its commercialization in the 2D realm.

The type of source precursors in bulk powder, transition metal oxide, or organic compound significantly impacts the growth temperature and the interface and optoelectronic properties. For example, though organometal needs a much lower temperature for the vapor phase transition, the carbon contamination is a significant outpouring in the synthesized material, detrimental to any device performance. However, bulk
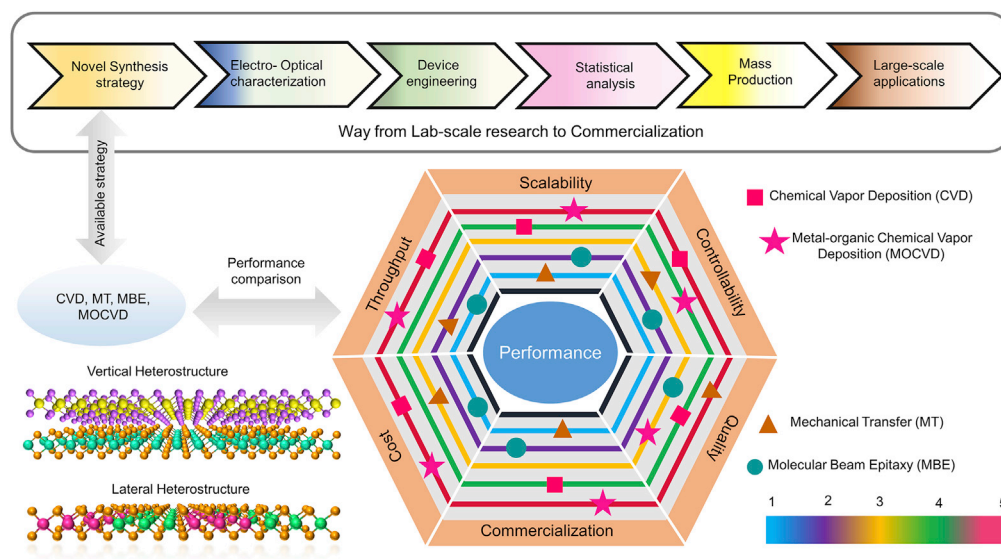
Figure 1. Roadmap toward commercialization
An overview of the roadmap for the commercialization of 2D technology and performance comparison (higher the point, better the performance) between the available synthesis strategies. CVD strategy is the most competent method to qualify as an unrivaled approach for fabricating 2D heterostructures. A schematic ball model of vertical and multi-junction lateral heterostructures is depicted.

transition metal chalcogenides as precursors require high temperature to overcome the solid-state barrier. Liquid phase source precursors are also favourable for high throughput with large area coverage of 2D HSs. However, accurate switching of liquid phase precursors, source contamination, and toxicity of most liquid phase precursors are still needed other strategies to overcome.

Vertical heterostructures (VHS)

TMD solid precursor. The CVD method has the potential in the design and assembly of TMDs layers without the constraints of epitaxy. Single-step CVD based-synthesis for TMDs HSs overcomes the difficulties of thermal degradation, surface oxidation of growth facets, and environmental exposure between each step which introduces unwanted impurities during the multi-step growth process. The single-step CVD method employs vapor phase precursors' selective evaporation and deposition from a heterogeneous mixture of solid sources. Usually, the mixed solid sources are placed inside a tube furnace between 700 and 1060°C, depending on the types of precursors, whereas the substrates are kept between 700 and 850°C for the deposition process. The deposition sequence of single and multi-junction HSs during the synthesis process is mainly controlled via growth temperature, growth time, rate of the reaction, molar ratio of TMDs components, movement of source material (back and forth), source to substrate distance, selection of carrier gases and gas flow rates (Duan et al., 2014; Gong et al., 2014; Huang et al., 2014; Sahoo et al., 2018). One-step growth of single-junction VHSs made of entirely different transition metals and chalcogenide has been shown as a potential step forward to obtaining a wide range of HSs. However, the degree of alloying, cross-contamination, and poor interface still requires further studies. Direct fabrication of multi-junction VHS via a one-step synthesis process has not yet been achieved because of the challenges involved in compositional alloying due to the coexistence of different vapors, the sensitivity of the pre-existing layer to different chemical environments, contamination, secondary reaction, and temperature-induced degradation. It is often required to aggressively change CVD growth parameters sequentially or swing the precursor back and forth, making this process tedious to accomplish. For VHS, controlling nucleation on the pre-existing 2D surface, lattice matching, and simultaneously creating a balance between vertical and lateral growth is challenging in the existing methods.

A recent report on the two-step epitaxial growth of monolayer WSe_2 and 2D topological insulators such as Bi_2Te_3 could produce a clean and sharp interface (Figure 2). The layer-dependent band alignment followed by a transition from type-II to type-III upon increasing the numbers of Bi_2Te_3 layers was appeared to be
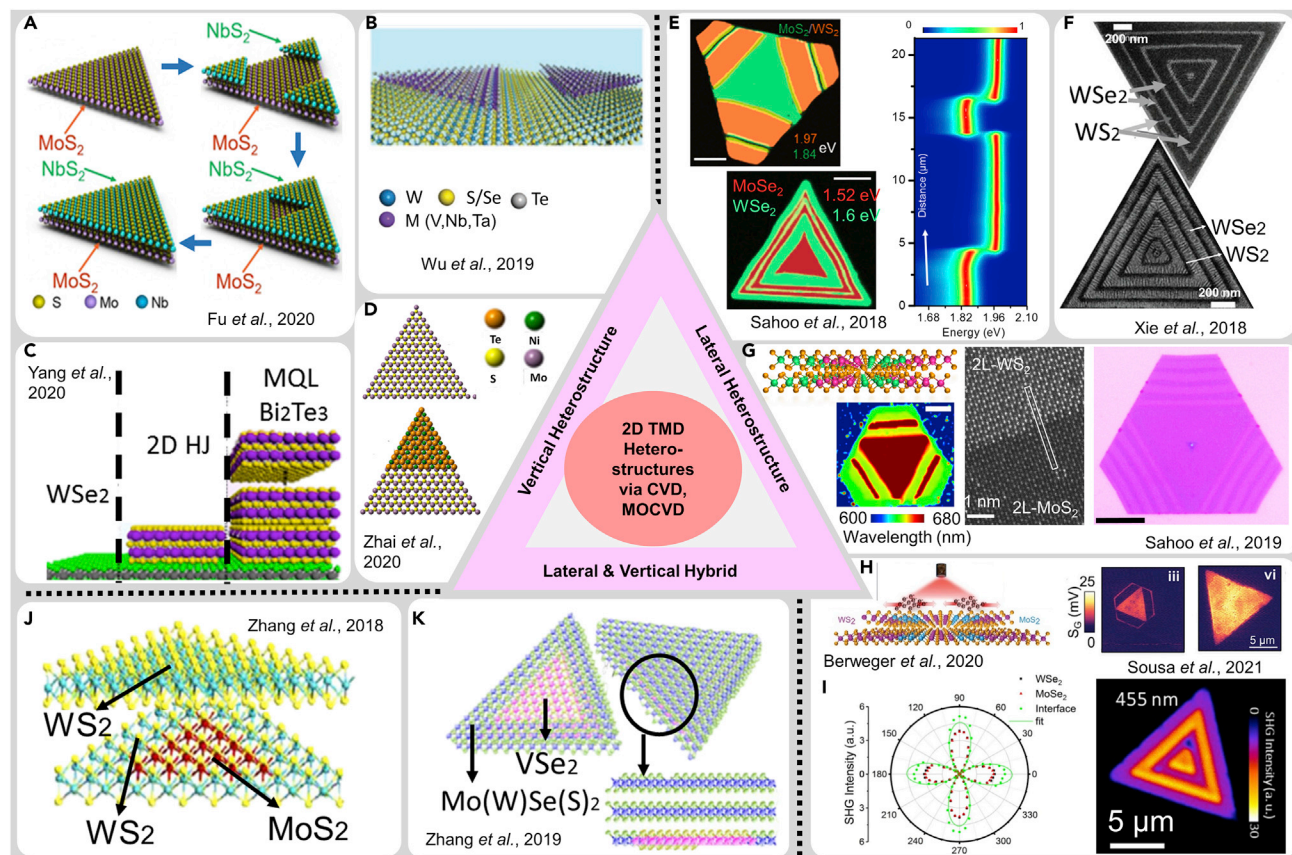
Figure 2. A brief overview of the recent progress made toward CVD growth of TMD HSs, including vertical, lateral, and hybrid configurations.

(A) A proposed growth sequence of NbS_2 on top of MoS_2. NbS_2 first nucleated at the corner on MoS_2 and migrated at the edges having full coverage of the bottom layer of MoS_2 (Fu et al., 2018). Copyright 2018, American Chemical Society.

(B) A schematic of a vertical MTe_2 (M = V, Nb, Ta) on the WX_2 (X = SE, S) layer (Wu et al., 2019c). Copyright 2019, Wiley.

(C) Schematic representation of multilayer Bi_2Te_3 on top of 1L-WSe_2 (Yang et al., 2020). Copyright 2020, American Chemical Society.

(D) Atomic ball model for $NiTe_2$/MoS_2 vertical heterostructure synthesized via two-step CVD process (Zhai et al., 2020). Copyright 2020, American Chemical Society.

(E) Composite PL-map of three-junction MoS_2-WS_2 (top left) and five-junction of $MoSe_2$-WSe_2 (bottom left) lateral heterostructures. Normalized PL contour plot (colored) along a perpendicular to the interfaces corresponding to the three-junction MoS_2-WS_2 (Sahoo et al., 2018). Copyright 2018, Springer Nature.

(F) SEM images of WS_2-WSe_2 superlattices (Xie et al., 2018). Copyright 2018, AAAS.

(G) Schematic for bilayer lateral heterostructure (top left). A PL position mapping (bottom left) and HAADF-STM image (middle) corresponding to MoS_2-WS_2 bilayer lateral heterostructure. An optical image of bilayer multi-junction MoS_2-WS_2 lateral heterostructure is shown with the scale bar of 10 μm (Sahoo et al., 2019). Copyright 2019, American Chemical Society.

(H) Persistence photoconductivity mapping of WS_2-MoS_2 multi-junction lateral heterostructure (left), and (right) microwave real part of conductance signal (S_G) of the channels with the increasing energy of excitation photon (1.75 and 1.97 eV) (Berweger et al., 2020). Copyright 2020, American Chemical Society.

(I) (left) Polarization dependence second harmonic generation (SHG) and (right) the corresponding SHG intensity maps of the single-layer $MoSe_2$-WSe_2 lateral heterojunction collected at 455 nm emission wavelength (Sousa et al., 2021). Copyright 2021, IOP.

(J) An atomic model of thin-film hybrid structure of WS_2/WS_2-MoS_2 (Zhang et al., 2018). Copyright 2018, IOP.

(K) Schematic of VSe_2 and TMDs hybrid structure where multilayer VSe_2 was grown at the edges of 1L-TMDs followed by coverage of top layer via two-step CVD process (Zhang et al., 2019b). Copyright 2019, American Chemical Society.

promising for self-powered photodetectors with faster response and a wide range of detection (Yang et al., 2020). The minor lattice mismatch between the Bi_2Te_3 on 1L WSe_2 induces a relaxed undistorted circular shape for the first quintuple layer of the topological insulator, which serves as the active nucleation cluster for subsequent growth along the vertical direction. However, high thermal stability and high diffusion barriers limit successive quintuple layers' growth to round edges with a truncated triangular shape. The conduction of the 1L WSe_2 can be modulated between p and n-type via changing the polarity of the gate bias. In VHS-based FET configuration, the Bi_2Te_3 layer is an effective protection layer with high work function.

In contrast, the WSe$_2$ domain shows a weak response to Fermi level pinning and chemical disorder which have advantages for efficient transport of carriers. Using the two-step CVD method, close to millimeter-sized WSe$_2$/SnS$_2$ bilayer VHS with a significant lattice mismatch of 14.3% can be synthesized using bulk TMD powder and SnO$_2$ at different growth temperatures. The size of individual domains can also be controlled (Yang et al., 2017). It was found that WSe$_2$/SnS$_2$ VHS formed a type-III broken-gap heterojunction in which respective domains behave as p- and n-type characteristics (Yang et al., 2017). This VHS exhibits low leak-off current (10^{-14} A), high on-off ratio (10^7), photoresponsivity of 108.7 mAW^{-1}, photodetectivity of 4.71 × 10^{10} Jones, and reasonable photoresponse time of 500 μs as compared to the pristine WSe$_2$ layer. Generally, in the two-step method, the initial 2D layer is prone to degradation before the growth of the second layer, mainly because of temperature-induced degradation. However, reversing the flow of carrier gases during the temperature ramping and cooling stages can protect the initial 2D layer. Based on this strategy, a bidirectional flow of Ar carrier gas was shown to be helpful for the growth of WSe$_2$/WS$_2$ VHS, where reversing the flow helped to resist the initial TMD domain from thermal degradation during the temperature ramping stage for the second layer growth, as well as it restricted the formation of undesired nucleation sites (Cao et al., 2020). However, the temperature of solid precursors used for this study was relatively very high (∼1160°C), which poses further issues related to the scalability of such a process.

Synthesis of tellurium-based TMDs VHS is limited because of the challenges of optimizing the reaction parameters via CVD. Their sensitive nature toward environmental degradation also needs to be resolved (Figure 2). Nevertheless, 1L WS$_2$ or WSe$_2$ has been used as the growth substrate for the synthesis of 2D metallic TMDs (MTe$_2$ where M = V, Nb, Ta) for the fabrication of MTe$_2$/WSe$_2$ (or WS$_2$) VHSs in a two-step CVD process using heterogeneous precursors for the growth of individual layers (Figure 2) (Wu et al., 2019c). Bulk TMD powders (temp ∼1180°C) were used to grow semiconducting domains. In contrast, transition metal chlorides such as NbCl$_5$, TaCl$_5$, or VCl$_3$ and tellurium power were used for the vertical growth of 2D metal layers in the temperature range of 540–610°C. It was found that the 2D-WS$_2$ layer was essential for the growth of atomically thin 2D metal layer; otherwise, thick transition metal telluride layers were obtained on SiO$_2$ substrates. This can be understood from the viewpoint of adatom migration rate, which can be expressed in diffusion rate $D \approx D_\infty \exp[-U/k_B T]$, where U is the energy barrier for the surface diffusion, T is the growth temperature, and k$_B$ Boltzmann constant. For the SiO$_2$ surface, a larger U suppresses adatoms' diffusion and promotes the formation of thick layers via vertical growth. The surface defect or trap states on the SiO$_2$ surface could also contribute to vertical growth. Whereas, smaller U for adatoms on dangling-bondfree flat WSe$_2$ (WS$_2$) surface ensured the quick diffusion of adatoms, leading to forming a thin MTe$_2$ layer.

In many cases, the nucleation of the second 2D layer occurs randomly. Focused laser irradiation (488 nm) combined with a raster scan created the localized periodic defects at specific positions on a single layer and bilayers semiconducting TMDs (WS$_2$, WSe$_2$, or MoS$_2$) to control the nucleation of the metallic-TMDs layer in the second stage of growth. Employing such a strategy, the site-specific controlled growth of various metallic-TMDs arrays of VS$_2$, VSe$_2$, NiTe$_2$, CoTe$_2$, or NbTe$_2$ were synthesised independently on semiconducting TMDs via two-step CVD methods, as mentioned above (Figure 2) (Li et al., 2020a). This method demonstrated that nucleation site, periodic arrangement, and tuneable lateral dimensions could be well controlled. Apparently, upon laser irradiation, first SE vacancies are created, leading to the formation of dangling bonds on transition metal (W or Mo) terminated surface. The adsorption energy of 2D metallic compounds such as VSe$_2$ at the W-terminated surface (−2.98 eV) is much lower than that of the pristine WSe$_2$ surface (0.16 eV). Therefore, it is much easier for the metallic TMD-related adatoms to nucleate at the patterned transition metal-terminated surface, forming a homogeneous metal bonded vdW interface across the VHS. The significant lattice mismatch of as-synthesized 1T VSe$_2$, NiTe$_2$, and CoTe$_2$ domains on 2D TMDs leads to the observation of moiré pattern with the periodicity of ∼14.7, 2.3, and 2.6 nm, respectively. Further optimization could be done to control the thickness of the top metallic layers and improve their stability. The formation of the leading 2D metallic layer could provide comparatively better charge transport characteristics because of the reduction of interfacial contact resistance. In addition, such VHS composed of heterogeneous TMDs with different lattice constants can form moiréincommensurate lattices that could host unique charge carriers, including moiré excitons.

Oxide precursor. Most CVD methods employing bulk TMDs as solid precursors required significantly elevated temperatures to evaporate (>1000–1180°C). However, transition metal oxide precursor possesses a relatively lower melting temperature and lower vapor pressure than the bulk TMD powder. Hence,

transition metal oxide precursors have been widely used to grow various TMDs and their heterostructures. VHS of WS_2/MoS_2 was initially reported in a facile one-pot CVD method where MoO_3 powder was used as a source of Mo-precursor along with a mixture of W and Te on the substrate as seed promoter. The difference between the nucleation and growth rates of MoS_2 compared to WS_2 helps the formation of HSs. The reaction temperature can be varied to control the growth of TMD domains either in the vertical (temperature of ~850°C) or lateral direction (~650°C). The lateral interface between monolayer MoS_2 and WS_2 was rough in this differential growth rate-limiting process because of the formation of thermodynamically preferred alloys. A two-step CVD strategy using transition metal oxide precursor was used to synthesize $WSe_2/MoSe_2$ VHS and their hybrids at ambient pressure (Gong et al., 2015). The growth temperatures were adjusted to 750°C and 900°C for the growth of $MoSe_2$ and WSe_2 domains, respectively. However, the interfaces were found to be alloyed and lacked long-range ordering. Growth along lateral or vertical directions can also be controlled using the sequence of the precursor supply in the CVD process (Heo et al., 2015). The sequence of W- to Mo- related precursor supply produces LHS, whereas reversing the supply of precursors promotes VHS. A temperature-triggered strategy for the growth of $MoSe_2/MoS_2$ HS either in the lateral or vertical direction was reported via oxide-assisted one-step APCVD (Chen et al., 2019). The flux rate of sulfur precursor and the distance of 10 and 5 cm between the source and growth substrates were also used to control lateral or vertical growth. The high flux of precursors favors the adatoms to easily overcome the hopping energy barrier along the vertical direction compared to the lateral direction. Growth of heterogeneous WS_2/MoS_2 VHS was also reported using a mixture of transition metal hydroxides $[(NH_4)_2MoO_4$ and $Na_2WO_4]$ and KOH or NaOH via the one-pot CVD method (Zhu et al., 2020). Initially, bilayer MoS_2-OH formed under Ar ambient, whereas changing the carrier gas to H_2 favored the formation of WS_2 domains. OH- passivates the top surface of the initial 2D domains at lower temperatures that promote LHS. At higher temperatures (850°C), the decomposition of WS_2 and OH facilitated the vertical growth of WS_2 on the initial MoS_2 layer.

Vertical hetero-epitaxy of narrow bandgap p-type semiconductor Sb_2Te_3 on 2D MoS_2 layer despite the significant lattice mismatch (25%) was reported in a two-step CVD strategy (Liu et al., 2019), where the MoS_2 layer was synthesized initially from MoO_3 precursor followed by the direct evaporation of Sb_2Te_3 bulk powder at 600°C. Such VHS shows good photo conversion efficiency (4.5%) and fast photoresponse time (<500 µs) as compared to conventional TMDs based devices. HSs composed of transition metal mono- and di-chalcogenide-based $GaSe/MoS_2$ p-n vertical and lateral junctions were reported via liquid gallium-assisted two-step CVD method (Zou et al., 2021). The growth direction of the GaSe layer was controlled by tuning the amount of Ga mixed with Ga_2Se_3 powder on the as-grown 1L MoS_2 layer. Selenium can easily be absorbed and pinned on the surface of the MoS_2 layer owing to the high diffusion barrier and most negative adsorption energy than the other possible reactants ($GaSe_3$, GaSe, Ga_2Se, and $GaSe_2$). The addition of Ga helps to form a GaSe molecule cluster having good diffusion ability on the MoS_2 surface. The unsaturated dangling bonds on the edges of the MoS_2 layer acts as the active nucleation site for GaSe. Maintaining a lower Ga/Se (~0.84) flux ratio, active clusters of Ga_2Se and $GaSe_2$ dominate the chemical environment and promote vertical epitaxy, owing to a high formation energy barrier of these reactants to cross the MoS_2 step edges. On the other hand, high Ga/Se (~1.25) ratio, GaSe molecule density increases, which has low Ehrlich-Schoebel barriers and diffuses toward MoS_2 edges, resulting in LHS formation. In such a growth process, the substitutions of sulfur atoms from the MoS_2 surface by selenium cannot be ruled out.

Bulk TMDs precursor-based one-, two-, or multi-step strategies are widely employed to synthesize VHS or multi-junction superlattice. One-step process is free from thermal and environmental degradation; two-step or multi-step suffers from that issue, but controllability is higher. Bulk precursor-based CVD growth needs higher temperature, a significant roadblock for its commercialization. Direct synthesis of vertical superlattice via one-step method is a challenge to encounter in the future via overcoming cross-contamination, secondary reaction, and thermal degradation issues. To reduce the growth temperature, one can use oxide precursors instead of bulk precursors. For VHS, higher growth temperature, higher adatoms flux, or low hopping barrier for incoming adatoms promotes the growth.

Single and multi-junction lateral heterojunction (LHS)
Bulk TMD precursors. Vertical heterostructures can be realized either by mechanical exfoliation or via direct growth. However, atomically stitching materials in the lateral direction is only possible via direct growth. The first successful synthesis of LHS of 1L $MoSe_2$-WSe_2 was carried out in a single-step physical

vapor transport method using a mixture of TMDs bulk powder counterparts as precursors (Huang et al., 2014). The difference in the volatility and vapor pressure of different TMDs precursors leads to the growth of $MoSe_2$ followed by the edge-epitaxy of WSe_2 domains. However, the TMD domains are susceptible to multiple exchanges of growth systems and chemical environments, which posed a challenging task for the sequential growth of multi-junction LHS.

Nevertheless, a reverse flow strategy was adopted to the conventional physical vapor transport system for sequential fabrication of heterogeneous TMDs LHSs, and superlattices via the multi-step process. TMD bulk precursors were directly used depending on the types of 2D domains in the LHSs. As a result, it was possible to realize different transition metal and chalcogenides-related components without forming alloys across interfaces by separating the growth chamber to synthesize constituent TMD domains (Zhang et al., 2017b). The monolayer multi-junction TMDs LHSs and lateral superlattices were also demonstrated under a bidirectional flow of carrier gases to mitigate the problem associated with uncontrolled nucleation during the temperature ramping stage and avoid cross-contamination during the exchange of precursors. Individual domains with the LHS were controlled by varying the growth temperature and reaction time. However, this bidirectional carrier gas-based strategy complicated the growth of multi-junction TMDs LHSs, and lateral superlattices. Moreover, this technique lacks scalability on account of multiple exchanges of growth chambers to fabricate individual domains.

Atomically thin TMD layers are prone to degradation during the multiple exchanges of growth processes. It is thus desirable for developing a growth strategy that can allow continuous and direct growth of multiple 2D layers without breaking the growth condition or exchanging CVD systems is the need of the hour for high-quality VHSs and LHSs. In this context, we recently reported a simple, scalable, robust, and highly reproducible water-assisted one-pot CVD method for the *in situ* growth of multi-junction LHSs with the precise number of 2D layers, the width of individual domains, degree of alloying, and atomically sharp interfaces, simply through changing the carrier gases (Figure 2) (Sahoo et al., 2018). A mixture of TMD powders at high temperature ($\sim$1060°C) was allowed to react with different carrier gases, whereas the substrates were placed in the temperature range of $\sim$750–820°C. The N_2 carrier gas through H_2O promoted the selective evaporation of Mo-related precursors leading to the formation of the MoX_2 domain, whereas switching to reducing gases such as Ar with H_2 (5%) stopped the growth of MoX_2 and promoted the nucleation of WX_2 domains. The novelty and simplicity of the above one-pot CVD method is the vapour-phase modulation induced *in situ* growth of multi-junction LHSs, which does not require any source switching or toxic precursors. Furthermore, the number of layers within the LHS can be controlled by adjusting the kinetic coefficient of adatoms, thereby fine-tuning the substrate temperature and amount of solid TMD precursor (Figure 2).

2D metal-semiconducting LHS composed of hexagonal WSe_2 (1 and 2L as a core layer) and tetragonal CoSe for realizing edge as well as ohmic contact, a way to reduce the contact resistance, was reported via a two-step vapor transport method where bulk WSe_2 powder was used for the growth of WSe_2 layer whereas $CoCl_2$ precursor was used for the growth of metallic layer (Ma et al., 2021). It was shown that growth temperature could impact the lateral size of the metallic layer as per the following trend; (i) rising growth temperature from 535 to 570°C significantly increases the lateral width of the 1L CoSe layer, and (ii) thickness of CoSe layer remain identical at the edge of 1L-WSe_2 with increasing the growth temperature whereas the thickness of CoSe layer increases on the edges of 2L-WSe_2. For such a system, the growth and diffusion rate of adatoms were influenced by a slight increase in the growth temperature. Lower growth temperature promotes the adatoms effectively diffusing toward the edges and contributes lateral growth, whereas high temperature favored the growth at the high energy sites forming comparatively thick layers.

Oxide precursors. Using transition metal oxides and chalcogen powder as precursors, WSe_2-$MoSe_2$ LHSs via a two-step CVD process was demonstrated in which substrate temperature was maintained at 750 and 900°C for the growth of $MoSe_2$ and WSe_2 domains, respectively. However, interface alloying and lack of long-range crystalline ordering can be seen owing to the difficulties in controlling the mechanism for the vapor phase precursors (Gong et al., 2015). Atomically sharp 1L WSe_2-MoS_2 LHS was synthesized in a two-step CVD method (Li et al., 2015), where the growth temperature for WSe_2 and MoS_2 were maintained at 925 and 755°C, respectively, under varying chamber pressure. The interface obtained in this process was sharp and pristine. Using a one-pot CVD process, compositionally tunable synthesis of LHSs of MoS_2-WS_2 (680–800°C), MoS_2-alloy (680–950°C), and alloy-WS_2 (840–950°C) types were reported by Lee

et al. using a mixture of different transition metal oxide precursors with ammonium hydroxide (NH_4OH). LHSs were synthesized directly via controlling (i) the time of S vaporization, (ii) growth temperature, and (iii) the concentration of metal oxide precursors. The vapor phase WO_3 precursors play a significant role in controlling the growth either in the lateral direction (low supersaturation of WO_3) or simultaneous growth along the lateral and vertical direction (high supersaturation level for WO_3 vapor) (Lee et al., 2019). Zhou et al. demonstrated sub–2-nm-wide quantum wells LHSs of MoS_2-$MoSe_2$ and WS_2-WSe_2 via two-step CVD growth where the first WSe_2 (or $MoSe_2$) layer was grown at elevated temperature followed by the growth of WS_2 (or MoS_2) domains (Zhou et al., 2018). Misfit dislocation-driven growth of quantum well LHSs can be explained with the three steps; (1) large lattice mismatch around 4 and 4.5%, respectively, leads to the formation of uniform tensile strain, which drives the formation of periodic dislocation at the junction, (2) these dislocations in the initial MoS_2 or WS_2 layer grows with time along the specific crystallographic direction, and (3) climb of the dislocations into WSe_2 (or $MoSe_2$) matrix is energetically favourable for the parallel growth of the quantum well along with the growth of LHSs. Generally, high temperature and a substrate with a rough surface can promote vertical and uncontrolled growth of TMDs with defective interfaces. Such issues can be addressed via a low-temperature synthesis process for the growth of LHSs. Temperature also plays a more significant role in scaling up the method toward hetero-integration of other 2D materials. Multi-junction LHS of 1L WS_2-WSe_2-MoS_2 domains were reported with minimal compositional fluctuation, low defect densities, and high interface qualities using atmospheric pressure APCVD for the initial WS_2 layer followed by a low-pressure CVD method in the subsequent growth steps (Chiu et al., 2018).

Growth of metal-semiconductor LHS composed of WS_2-ReS_2 (2H-1T') was demonstrated with a defect-free interface via an H_2-triggered one-step CVD method using a mixture of metal oxide precursors (Liu et al., 2020). The first ReS_2 layer was grown under the Ar atmosphere, followed by the lateral growth of the WS_2 layer at the vertices of ReS_2 by changing the carrier gases from Ar to a mixture of Ar + H_2. The addition of H_2 reduces the volatility of Re_2O_5 as an intermediate phase during the reduction process of the ReO_3 precursor. Subsequently, it forms a metallic Re layer which stops the supply of Re-related precursors. Meanwhile, the growth of the WS_2 layer was promoted in the presence of the H_2 atmosphere. However, the hetero-phase junctions are irregular because of the significant lattice mismatch that requires further studies.

Generally, higher evaporation temperature is needed for many transition metal compounds for which salts such as NaCl or KCl effectively reduce the growth temperature and yield. In salt-assisted TMDs HS growth, different intermediate volatile oxyhalides form, which is subsequently transported to the growth substrate and help the growth of TMD domains at relatively lower temperatures ($\sim$700°C for MoS_2 and $\sim$850°C for WS_2) (Chen et al., 2015; Wang et al., 2017). Zhang et al. reported using perylene-3,4,9,10-tetracarboxylic acid tetra potassium salt (PTAS) as nucleation seeds as the growth promoter to realize TMD LHs (Zhang et al., 2015). However, further studies are desirable to evaluate the exact role of such growth promoters and their influence on the structural, optical, and device properties of many TMDS based HSs.

Metal-organic precursor. Most of the transition metal-based bulk or oxide precursors need a significantly high temperature to synthesize various TMDs based HSs, which further poses issues related to scalability and reproducibility. The advantage of using the metal-organic compound for transition metal precursors is their low evaporation temperature compared to conventional bulk transition metal precursors. The growth of different TMDs via the MOCVD process can provide a stable growth environment for wafer-scale 2D TMDs. Few recent reports demonstrate its capability to grow multi-junction LHSs superlattices (Kobayashi et al., 2019; Xie et al., 2018). Coherent growth of 1L WSe_2-WS_2-WSe_2 and WSe_2-MoS_2-WS_2 LHS-based superlattices were demonstrated via the salt-assisted MOCVD method by simultaneously changing the organometallic and chalcogenide precursors as per the requirement (Figure 2) (Xie et al., 2018). The width of TMD domains within the superlattice can be fine-tuned by adjusting the switching time between precursors. However, most of the structures demonstrated in this process resulted in considerable strain in TMD domains, making these materials prone to environmental degradation. Strain-free synthesis of multi-junction LHS is necessary to evaluate the optoelectronics characteristics in lateral geometry and improve the device stability. Growth multi-junction LHS composed of WS_2-MoS_2-WS_2 on graphite substrate was also synthesized in an MOCVD method using metal-organic precursors (Kobayashi et al., 2019). The advantage of the MOCVD method is the possibility of simultaneous change of transition metal and chalcogenides domains without a significant degree of alloying across interfaces and have the potential for scalability.

Like VHS, LHS is not possible via mechanical transfer technique due to lattice matching constraints. In contrast, direct LHS or multi-junction lateral superlattice synthesis is possible via single-step, two-step, or multi-step strategies with bulk or oxide precursors. The performance tradeoff between each method follows VHS growth. Compared to VHS, low growth temperature, low incoming adatom flux, or high hopping barrier favors LHS growth. In context to CVD, MOCVD is also emerging as a scalable and potential approach to growing LHS with controlled interface width and lower evaporation temperature of precursor that make it exciting for commercialization.

Mixed lateral with vertical hybrid structures

Bulk sources. Bulk solid sources of TMDs materials are also sensitive to humidity during the reaction time at high temperatures, producing complex oxides and hydroxides. The presence of such oxide species can reduce the growth temperature. Gypsum [$CaSO_4.2H_2O$] has been reported as a solid water source to control the vapor pressure inside the CVD reactor. Controlling the thermal decomposition of the water source present inside the CVD reactor, a one-step vapor transport-based growth of complex HSs with lateral, vertical, and hybrid MoS_2-WS_2 hetero-interface was reported (Zhao and Jin, 2020). For the initial WS_2 layer deposition, a lower temperature of the water source ($\sim$85°C) was maintained, which resulted in a low amount of vapor phase precursor and, hence, lower supersaturation of WS_2 particulates. In addition, it promotes screw dislocation resulting in the formation of spiral WS_2 nanoplates. On the other hand, the higher source temperature of the water source ($\sim$120°C) invoked layer-by-layer deposition of WS_2 with a large lateral dimension. Subsequent growth of the MoS_2 layer along the edges of the pre-deposited WS_2 layer gives rise to the formation of LHS composed of single or multiple layers depending on the size of the pre-deposited WS_2 layer. At the initial stage, the WS_2 layer of different sizes first formed. With the prolonged reaction duration, another layer of MoS_2-WS_2 fully covers the bottom MoS_2-WS_2 LHS rising a hybrid-like structure.

Oxide source precursors. A hybrid HS consisting of lateral with vertical growth direction (WS_2/MoS_2-WS_2) was reported in a single-step CVD method by adjusting the growth temperature and flow direction of carrier gas (Figure 2) (Zhang et al., 2018). Initially, 1L MoS_2 formed because of the low submission temperature, followed by the formation of the WS_2 layer at the edges of the core MoS_2 layer, predominantly in a hexagonal or triangular shape. Further increasing the temperature (>850°C), the adatoms gain enough energy to overcome the energy barriers and contribute to vertical growth, in the form of a second WS_2 layer that partially or fully covers the initial MoS_2-WS_2 LHS. At higher temperatures, simultaneous growth along lateral and vertical directions became more kinetically favourable.

Direct growth of 2D Metal–Semiconductor-based lattice-matched multilayer metallic IT-VSe_2 on 1L 1H-MX_2 HS was demonstrated via the two-step CVD method (Figure 2) (Zhang et al., 2019b). During the initial stage of nucleation, the VSe_2 layer preferably formed an edge-elongated stack along the edges of 1H-MX_2, which eventually merged, leading to the completion of the vertical layer. The significant difference in the diffusion of VCl_3, a source VSe_2, and transition metal oxide precursors

Prevent the formation of the alloy during the second growth step. The small lattice mismatching between different 2D layers, lattice misfits of $\sim$2.2 and $\sim$1.9% for VSe_2/WSe_2 and VSe_2/$MoSe_2$, respectively, leads to the formation of commensurate lattice stacking along the vertical direction. The possible reason for such growth behavior of the VeS_2 layer could be the choice of substrate and growth template. The dangling bonds on the sapphire surface impede the outer lateral growth mode, whereas the dangling bond-free top MX_2 surface is much easier for metallic VSe_2 layers to grow.

The lattice structures of transition metal mono-chalcogenides in MX-type are different from MX_2 type TMDs. Hence, HSs composed of MX/MX_2 structures are expected to form incommensurate lattices such as Moiré patterns with unusual physical phenomena. However, LHS between heterogeneous layered materials with large lattice misfits would be challenging to synthesize via the CVD method. Nevertheless, hybrid HSs composed of 2D GaSe and $MoSe_2$ (lattice mismatch $\sim$13%) both in lateral and vertical directions were reported using a two-step lower pressure CVD method using MoO_3, Se, and a mixture of GaSe + Ga_2Se_3 powder as precursors (Li et al., 2016b). Single-layer GaSe was directly deposed on the CVD-grown $MoSe_2$ layer by adjusting the carrier gas flow rate. At a low flow rate, the vapor phase deposition of GaSe is slower than the diffusion on the substrate. In addition, the diffusion barrier of GaSe on the $MoSe_2$ layer is lower than the absorbance energy of GaSe molecule on the SiO_2 substrate, which leads to the deposition of
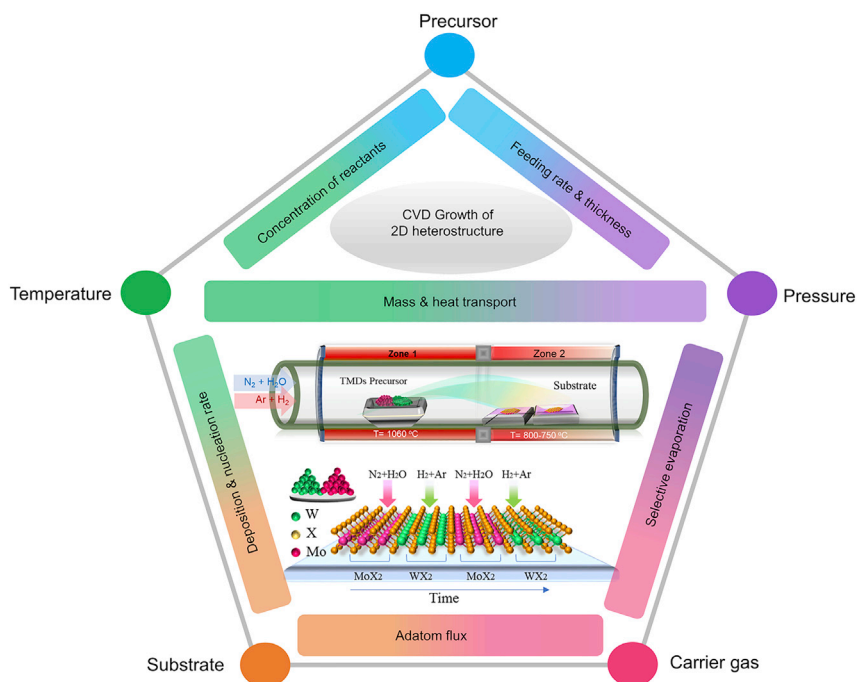
Figure 3. Growth controlling CVD process parameters
Schematic representing how different CVD process parameters (precursor, temperature, substrate, pressure, and carrier gas) affect the thermodynamics and kinetics of incoming adatoms in the CVD growth of 2D heterostructures.

GaSe on the MoSe$_2$ terrace and slowly covers the entire MoSe$_2$ surface. With increasing the flow rate, the deposition rate dominates over the diffusion rate, which increases the number of nucleation sites and promotes the growth along the lateral direction. Large lattice misfit leads to the observation of rough interfaces and the vertical and lateral directions. Compared to LHS, the vertical p-n junction (GaSe as p-type and MoSe$_2$ as n-type) exhibited strong photovoltaic characteristics. Further studies are desirable to understand the role of other growth parameters such as temperature, pressure, and flux ratios toward controlling the interface characteristics. In addition to vertical and lateral HS, its integration into a hybrid structure shows exciting functionalities. Its direct CVD growth is reported via single and two-step methods using bulk and oxide precursors. The tuning of humidity environment, growth temperature, flow rate during reaction time promotes vertical or lateral growth direction that eventually forms a hybrid structure.

Growth mechanism of heterostructures

Although several breakthroughs have been made to understand the growth kinetics for TMDs based HSs, concrete and universal growth mechanisms are still lacking for further progress in this direction. It depends on several crucial parameters, including growth temperature, growth environment, types of precursors, precursor's physicochemical properties (purity, evaporation-temperature, evaporation rate, nucleation rate, vapor pressure, volatility), adatoms flux ratio, precursors to substrate distance, sequence of precursor, substrates, and types of carrier gases within the CVD reactor (Figure 3). In the following section, a comprehensive discussion of different possible growth mechanisms proposed to date has been outlined to help the researchers take appropriate steps while controlling other CVD parameters during the growth of 2D HSs.

Vertical and lateral selective growth

Competition between thermodynamic and kinetic factors during the growth of HS is the main driving force to detect the shift in either vertical or lateral direction, apart from other physicochemical and CVD process parameters (Gong et al., 2014) (Figure 3). The energies gained during the growth of LHS and VHS, attributed to edge-binding/chemical bonding and vdW interaction, can be estimated via the following equations.

$$\text{Edge energy (for lateral Growth)} = \alpha L$$

$$\text{van der Waals Energy (for vertical Growth)} = \frac{\sqrt{3}}{4}\beta L^2$$

It indicates that the edge-binding and vdW energies are linearly correlated with contact length and contact area, respectively. The proportionality constants α and β represent energies gained per unit length and area, respectively, because of chemical bonding and vdW stacking during growth. Using density functional theory simulation, the typical values of these constants are found to be $\alpha = 1.62$ eV/Å and $\beta = 0.026$ eV/Å^2 for MoS_2-WS_2 HS. Higher contribution of the factor α than β, indicating a significant difference between the energies gained during the growth in the lateral and vertical direction at a fixed edge length (L), which becomes even more critical with increasing L. It indicates that the vertical stacking is thermodynamically favorable at a relatively higher temperature ($>800°C$) than lateral growth. At somewhat lower temperatures ($650–750°C$), low nucleation and growth rates of WS_2 domains make the process extremely difficult for the incoming adatoms to sit on the surface of the MoS_2. Instead, they can easily attach to the edges of the pre-existing MoS_2 via chemical bonding that needs much smaller nucleation energy and hence facilitate lateral growth. Apparently, at a relatively higher temperature, the thermal energy for adatoms becomes sufficient to overcome the nucleation energy barrier in the vertical direction to promote more thermodynamically stable VHS, where the kinetic effects turn out to be insignificant. On the other end, at relatively lower temperatures, kinetic effects dominate over thermodynamic factors that facilitate lateral growth. Without controlling growth direction via temperature selective thermal evaporation, vertical and lateral selective growth can be achieved via tuning vapor concentration of the solid source by controlling its position within the CVD reactor. Vertical and lateral HSs of MoS_2 and $MoSe_2$ monolayers were reported via a one-pot CVD method under ambient pressure using MoO_3, Se, and S powder as source precursors (Chen et al., 2019). The carrier gas (mixture of Ar and H_2) facilitated the formation of the initial $MoSe_2$ layer, followed by the growth of the MoS_2 layer on the pre-existing edges or top of $MoSe_2$ depending on the position of the S powder in the furnace placed upstream. The competition between diffusion and deposition rates can decide the growth direction. However, appropriate control on the selective evaporation of S and Se usually leads to irregular layers and poor controllability of HS's shape, size, and layer number. Apart from temperature and vapor-concentration favored growth, stringent control on nucleation sites plays a vital role in the selective growth of HSs. The hydroxide-assisted one-pot method can offer strict control on the nucleation sites to realize the optional formation of VHS and LHS. Zhu et al. (Zhu et al., 2020) reported synthesizing WS_2 by MoS_2 stitching and WS_2 on MoS_2 stacking HSs via hydroxide mediated one-pot strategy. However, OH^- is not desirable toward its practical employment for device fabrication. It can act as a scattering center and charge trap, which subsequently lowers down efficiency and speed of the devices. To overcome the selective evaporation issues in the temperature selective one-step method, using sequential vapor-phase reactants transport, the growth of monolayer MoS_2-WS_2 LHS and WS_2/MoS_2 VHS can be selectively controlled via temperature using two-step CVD (Heo et al., 2015). The mechanism behind this deterministic growth of monolayers into stitching or stacked heterostructures can be explained in the classical nucleation kinetics model framework. During the growth of the second TMD layer via selective incorporation of incoming vapor reactants, the initial as-grown layer on the substrate acts as active nucleation sites for the incoming adatoms, which can follow two paths; either the edge nuclei of the second layer can wet the first monolayer's surface (thus favored stacking) or wet the substrate (yield lateral stitching). The path selection is determined thermodynamically by energy-barrier for nucleation (ΔG^*) at a fixed growth temperature. According to the classical nucleation kinetics, change in Gibbs-free energy during nucleation at a hetero-interface is a function of nucleus radius (r) and difference in surface-energies between the substrate and nucleus ($\gamma_c + \gamma_{sc} - \gamma_s$). For a disk-shaped nucleus of monolayer crystals, this change can be expressed as follows:

$$\Delta G\ (r,\ \gamma)\ =\ \pi r^2 t\Delta G_V +\ \pi r^2\ (\gamma_c + \gamma_{sc} - \gamma_s)\ + 2\pi r t \gamma_{c,edge}$$

where r and t, γ_c, γ_{sc}, γ_s and $\gamma_{c,edge}$ corresponds to the radius and thickness of the nucleus, surface energy of the substrate, surface energy of the nucleus of monolayer crystals, interfacial energy between the substrate and nucleus, and surface energy of the nucleus edge of monolayer crystals per unit area, respectively. Whereas ΔG_v is the change in free energy per unit volume during nucleation. Therefore, the first term in the equation is the volume free energy change, and the last two terms are the surface free energy changes during nucleation. The maximum value of ΔG represents the free energy barrier (ΔG^*) for nucleation, and it turns out that $\Delta G^*_{lateral} > \Delta G^*_{vertical}$ during the sequential exchange of precursors. Generally, the associated nucleation rate (R) follows a trend in which R is maximized at a higher T_{growth} for smaller ΔG^* (VHS) or vice-versa.

Lateral heterostructure (LHS) growth

The variation in vapor pressure of gas-phase precursors because of their volatilities can enable the growth of different TMDs at different times, which eventually leads to the formation of LHS without changing any other parameters. To avoid the detrimental role of exposure to the ambient environment, *in situ* modulation of vapor components via *in situ* source switching (Duan et al., 2014) can fulfill the motive. In this method, the outer layer is grown via the attachment of the incoming adatoms to the outlying unsaturated edge-dangling bonds of the initial core layer that act as active nucleation sites. However, this strategy suffers from the detrimental effects of the break-in initial growth process and buffer time to attain the favorable growth environment of the second material. To encounter this limitation of the two-step strategy, Sahoo et al. developed a unique water-assisted one-pot strategy to synthesize large-scale HSs (Figure 3). Simplicity, high optical and electronic grade sample output, and the ability to fabricate single and layered controlled multi-junction HSs make the one-pot, water-assisted CVD method a robust, cost-effective, and promising strategy. Controllability over different TMDs and *in situ* sequential growth by simply switching to different carrier gases, without the prerequisite to exchange sources or reactor make this synthesis strategy advantageous to push this field onestep closer to commercialization (Sahoo et al., 2018). In this method, bulk powders of different TMDs can be used together directly to synthesize the LHS of respective materials. MoX_2 and WX_2 bulk materials partially converted to different Mo- and W- based oxide phases with different degrees of volatility during interactions with water vapor as oxidizing agent and H_2 as reducing agent at $\sim1060°C$ temperature is the critical factor behind the selective deposition of transition-metal components. In the presence of water vapor, the overall oxidation of MoX_2 led to the formation of the MoO_2, which sublimated rapidly at $1060°C$ and, subsequently, the vapor reactants transported to the desired substrate located at temperatures ranging from 700 to $810°C$, which further saturated on the substrate at those low temperatures. These re-condensed MoO_2 vapors then react with the existing chalcogen by-product such as H_2X, leading to the formations of MoX_2 domains. On the other end, during the interaction of WX_2 with water vapor, different W-related sub-oxide phases were evolved, which were only accumulated on the surface of the precursors in the presence of water vapor and did not participate in the growth process during the formation of MoX_2 domains. After prolonged interaction with H_2O, the growth of the MoX_2 domain was abruptly terminated by only switching the carrier gas *in situ* from H_2O to H_2 (5%) and promoting the growth of WX_2 domains at the pre-existing MoX_2 growth front. Therefore, using this unique way (*in situ* carrier switching), different multi-junction LHSs, superlattices, and their ternary alloys-based LHSs can be synthesized with better controllability and larger domain sizes, the number of layers, and minimal complications. The atomically sharp nature and the coherence among crystallographic orientation of different 2D domains of the as-grown LHS can be tracked via polarized resolved second harmonic generation (Sousa et al., 2021).

Hybrid growth directions: lateral and vertical (LHS + VHS)

The competition between the thermodynamic and kinetic factors to decide the growth direction in TMDs HSs is yet to be validated systematically (Figure 3). Under mass-driven kinetic reactions, a symmetric linear relationship is expected by the crystalline domain size with the amount of incoming adatoms flux of source precursors. However, such a symmetric trend was not observed by Sahoo et al.; instead, they found the promotion of vertical growth at elevated precursor concentrations (Sahoo et al., 2019). Further increase in concentration and hence adatom flux leads to the breakdown of self-limiting growth that decreases the domain size and facilitates the formation of the uncontrolled multilayer domains. Typically, it is convenient to assume that the substrate placed downstream will experience different temperatures at different positions in thermal CVD systems, following the furnace temperature profile. However, vapor-phase precursors also have a concentration gradient, which increases as the source to substrate distance decreases. Following these critical parameters, bilayer multi-junction LHSs can be obtained precisely by reducing the substrate to precursor distance and maintaining a temperature of $\sim820°C$.

In contrast, monolayers LHSs can be synthesized by further increasing the distance of the substrates from the precursor with a temperature below $800°C$. It stipulates that for layer-controlled growth, temperature plays a crucial role; lower temperature favors lateral growth, whereas higher temperature promotes vertical growth. This behavior of heterostructure can be understood from a multi-scale model in which the ratio of kinetic coefficients ascribed to attachment (K_{n-}) and detachment (K_{n+}) of adatoms at the edges of the pre-developed layer (n) is related to the growth-temperature (T_{growth}) via the following equation.

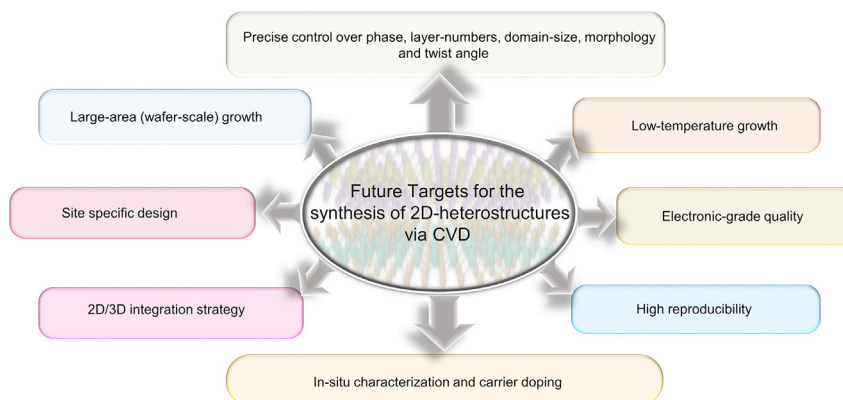$$K_{n+} = K_{n-} \exp\left(-V_b/k_B T_{growth}\right)$$

Figure 4. Future targets
Proposed future goals for the current state-of-the-art technology of the CVD method for the growth of 2D heterostructures to push the fascinating 2D physics into real applications.

where V_b is the energy barrier for the incoming adatoms to move between the bottom and top surface of the pre-existing layer. At relatively low temperatures (700–780°C), lack of sufficient energy to overcome the edge-energy barrier ($K_{n+} << K_{n-}$) compels the incoming adatoms to form stable covalent chemical bonds at the edges of the grown film, resulting in monolayer LHS. At relatively higher temperatures, as K_{n+} approaches K_{n-} ($K_{n+} \sim K_{n-}$), the incoming adatoms gain sufficient energy to hop across the energy barrier, promoting growth in both lateral and vertical directions simultaneously, resulting in a multilayer LHS. Further systematic studies are still desirable to accurately access the role of other mesoscopic CVD parameters that could be controlled to develop a comprehensive understanding toward simultaneous growth of LHS and VHS and HSs composed of a diverse class of layered transition metal compounds, bound conventional TMDs.

Future targets

For the past few years, scalable synthesis of 2D materials and heterostructures has been gaining tremendous research interest among the 2D research community to accelerate the path toward 2D technology-based next generation of intelligent electronics and optoelectronics devices aiming to fulfill the demand for sustainable Internet of Things (IoT) devices, energy, computation, sensors, and intelligent life. However, there is much room to optimize the current CVD strategy to enter real-world applications. To date, the lateral dimension of the flakes is limited to several hundreds of μm. For large-scale applications, wafer-scale samples with electronic grade quality are the stringent requirements for designing high-performance devices. Also, the existing CVD strategies need to be revised to get precise control over thickness, morphology, rotational alignment to explore new physics and new devices.

Furthermore, reproducibility is a big issue that needs to be solved with a strong effort for low-temperature growth. For next-generation applications, strategies capable of 2D/3D integration and site-specific design could be a promising way. The future targets for CVD are listed in Figure 4, to be achieved in the forthcoming years to drive 3D to the 2D paradigm shift. Dedicated efforts are anticipated for the large-scale integration of 2D HSs and the hetero-integration of 2D devices with existing Si-based technology for scalable applications in the coming 10–15 years to fulfill the targets to enter into quantum technology.

EXCITONS IN TMDS BASED HETEROSTRUCTURES

Excitons, the coulombic bound pairs of electrons and holes in TMD monolayers and their heterostructures have engrossed enormous research interest over the past decade because of unprecedented control on optical response stemming from out of plane quantum confinement and reduced dielectric screening. TMD family (monolayers and HSs) harness the excitonic landscape with unusual variants, including intra-layer exciton (IAX), bright and dark exciton, interlayer exciton (IEX), exciton complexes (biexciton and trion), and Moiré excitons. In general, excitons in TMDs possess large binding energy up to several hundreds of meV (Chernikov et al., 2014), compared to 3D semiconductors (~4 meV for GaAs), making them stable at

room temperature. The large binding energy of this quasiparticle in the monolayer regime attributed to a significant drop in dielectric screening and quantum confinement effect open the door toward novel exciton assisted 2D electronics, optoelectronics, and nano-photonics soon. Apart from these, electron and hole-based excitonic complexes such as trions having a finite angular momentum can be coupled with the rotational optical phonon of the substrate to form a new class of quasiparticles named polaronic trions whose binding energy can be tuned via crystallographic orientation (Trushin et al., 2020). Thus, the 2D semiconductors can pave the way to a pool of unconventional energy-quasiparticle via unconventional substrates.

Intralayer exciton (IAX)

The single-layer TMD shows strong light-matter interaction on optical excitation owing to reduced dimensionality, layer-dependent bandgap, and strong spin-orbit splitting. Strong in-plane coulombic interaction in monolayer limit, in conjunction with strong light-matter interaction, gives rise to intralayer exciton (IAX) in which both the members (electron and hole) are in the same layer. IAXs are classified into bright and dark excitons depending on optical accessibility. Spin-orbit coupling in TMDs leads to conduction band-splitting into two spin-polarized sub-bands with opposite spins. IAXs with electron and hole having a parallel spin and same k-value are optically accessible, which means they can easily recombine with a direct emission because of spin-momentum conservation, and are hence named bright excitons. On the other hand, IAX with electrons and holes having opposite spin or different k-values are optically inactive as photons cannot flip the spin or momentum and are termed dark excitons. Dark excitons are of two types: "spin forbidden but momentum direct" and "momentum forbidden but spin allowed". The lowest energy optical transition is spin allowed for molybdenum-based monolayers. In contrast, it is spin forbidden for tungsten-based monolayers owing to reversed energetic order of spin-polarized sub-bands.

Optically selective valley population and spin-valley locking in TMD monolayer provide additional valley degree of freedom, making them potential candidates for valleytronics application. However, the short lifetime ($\sim$2 ps) (Robert et al., 2017) and tens of picosecond valley polarization lifetime (Mai et al., 2014) of bright exciton pose difficulties for practical applications. Furthermore, spin-momentum violation makes direct exciton unable to take part in the optical transition to lower laying energy states and facilitate a longer radiative lifetime in nanosecond scale (Tang et al., 2019), which also be tuned by magnetic field and temperature to a microsecond (Jiang et al., 2018). Nevertheless, the presence of dark-excitons is expected to make TMDs a potential candidate to function as qubits (Maragkou, 2015) for optically controlled data coding, encoding, and transport (Zhou et al., 2017).

Interlayer exciton (IEX)

There is an abundance of TMDs HSs with type-II band alignment, where the conduction band minima and valence band maxima are in two different monolayers and support ultra-fast charge transfer. In this process, the electron or hole tunnel to the minimum or maximum available energy position, respectively. Before the recombination of charge carriers in IAX, formed after optical excitation in one TMD monolayer, the ultra-fast charge transfers (Hong et al., 2014) aid the formation of IEX with electron and hole in two different layers bound by long-range coulombic attraction. IEX was first observed in $MoSe_2$/WSe_2 vdW HS with a lifetime of 1.8 ns (Rivera et al., 2015), much longer than IAX ($\sim$130 ps) because of the slight overlapping of electron and hole due to spatial separation. IEX possesses lower binding energy compared to IAX as a result of spatial distribution in two different layers that enhanced dielectric screening. The long-lived ($\sim$100 ns (Miller et al., 2017)) IEXs with prolonged valley polarization (Kim et al., 2017), tunable excitonic emission via electric field due to the presence of directional dipole[8], dipolar interactions (Li et al., 2020b), and potential to switch the polarization of incoming light via electrical control (Ciarrocchi et al., 2019) are appealing features for applications toward photovoltaic, nanolaser, photonic, valley-based quantum information processing, and exploring quantum many-body systems. Excitons are bosonic particles with a much lower effective mass than ultracold atomic gas. The Bose-Einstein condensate (BEC) phase can be realized at a higher temperature. While a short lifetime of IAX restricts its condensation, the condensate phase of IEX in bilayer quantum well and bilayer graphene separated by h-BN layers have been observed under a high magnetic field at ultra-low temperature. Recently the macroscopic quantum phase has been observed in $MoSe_2$-WSe_2 hetero-bilayer isolated by few-layer h-BN at 100K (Wang et al., 2019c). Evidence of the IEX BEC phase at high temperature will drive researchers to explore exciton condensation-assisted optoelectronics applications and the realization of superfluidity (Fogler et al., 2014). Tunable-diffusion of exciton flux
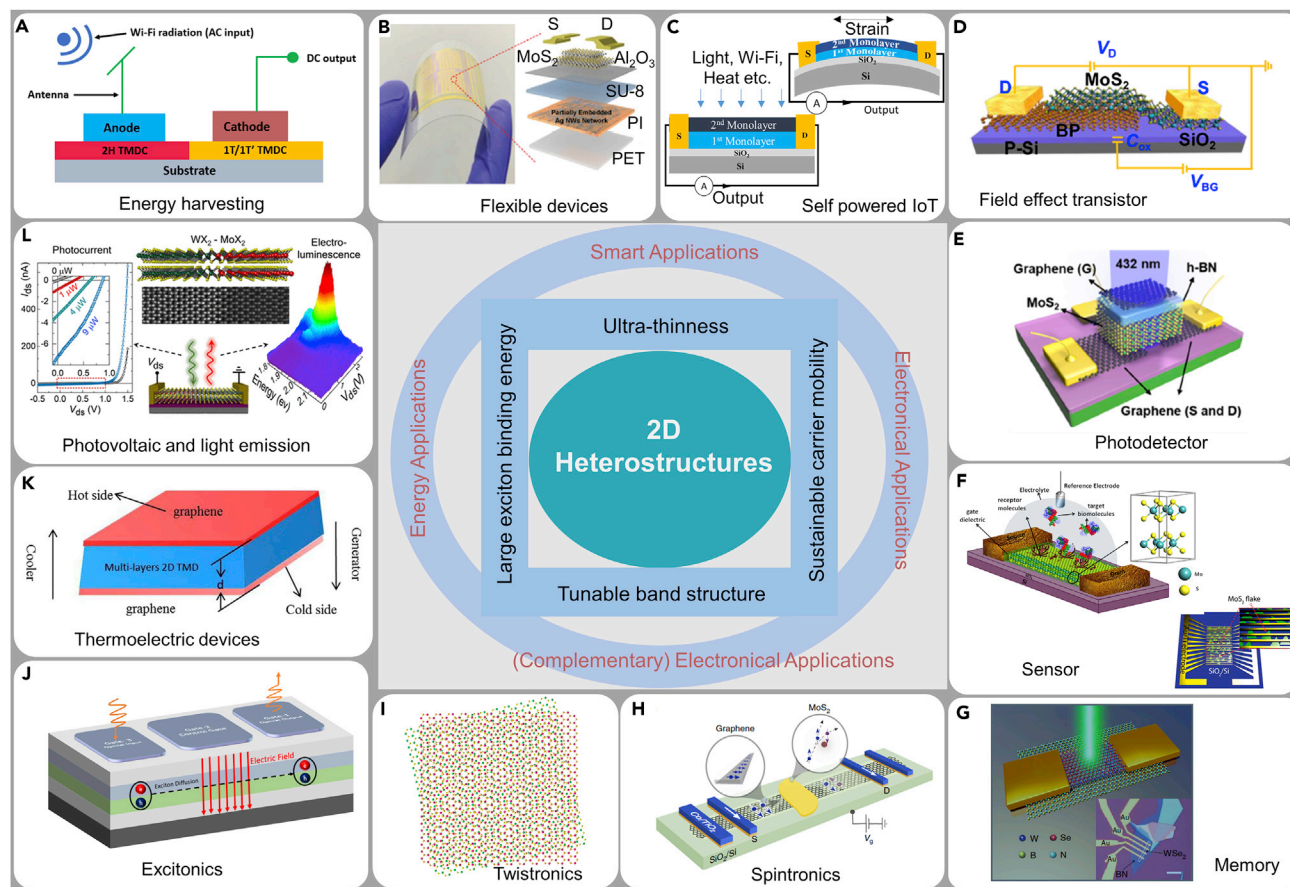
Figure 5. Potential applications of 2D materials based heterostructures

(A) Schematic representation of the semiconductor-metal junction-based 2D TMDs device for harvesting wi-fi signal (Zhang et al., 2019a). Copyright 2019, Springer Nature.

(B) MoS_2 based TFET arrays for flexible electronics (Song et al., 2016). Copyright 2016, Wiley.

(C) Schematic representation of next-generation sustainable IoT devices.

(D) Device schematic of MoS_2/BP heterostructure for FET operation (Liu et al., 2017). Copyright 2017, American Chemical Society.

(E) Graphene/MoS_2 Heterojunction based phototransistor for photodetection (Lee et al., 2020). Copyright 2020, American Chemical Society.

(F) MoS_2 based FET for bio and chemical sensing (Cho et al., 2015; Sarkar et al., 2014). Copyright 2014; 2015, American Chemical Society.

(G) WSe_2/h-BN heterostructure-based optoelectronic memory devices can discriminate wavelengths in the full visible spectrum (Xiang et al., 2018). Copyright 2018, Springer Nature.

(H) Schematic of graphene/MoS_2 heterostructure channel with FM source and drain contacts (Dankert and Dash, 2017). Copyright 2017, Springer Nature. The 2D structure allows spin injection from source, spin transport, spin manipulation, and detection of the spin signal.

(I) Manipulation of electrical and optoelectrical, and excitonic diffusion via controlling twist angle between two layers in vdW HS.

(J) Schematic of the 2D vdW HS for exciton-based switching application.

(K) Multilayer 2D TMD/Gr based thermoelectric devices in which temperature gradient between two graphene layers generate a voltage across TMD stacks (Liang et al., 2017). Copyright 2017, Springer Nature.

(L) Photovoltaic effect and room temperature electroluminescence response from bilayer MoX_2-WX_2 lateral heterostructure (Sahoo et al., 2019). Copyright 2019, American Chemical Society

controlled by electrostatic gating (Unuchek et al., 2018) and valley-polarized exciton current in excitonic circuits (Unuchek et al., 2019) can unlock a new paradigm, 'Opto-excitonic' in 2D applications (Figure 5J). However, the goal is limited to fundamental studies; developing an ideal CVD strategy can turn this phenomenal feasibility into real applications.

Moiré exciton & moiré superlattice

As the atoms sit at the surface of an atomically thin 2D film, it is possible to tune their electrical and optical responses without changing their chemical composition. One of the promising ways is the vertical stacking

of 2DLMs monolayers with identical or close lattice constants and/or angular misalignment that introduces a new periodicity referred to to as moiré superlattice. Interest in moiré superlattice of 2DLMs is gaining momentum with the observation of van Hove singularities (Ohta et al., 2012), Hofstadter's butterfly state and fractional quantum hall effect (Dean et al., 2013), gap opening at Dirac points (Wang et al., 2016), and moiré wavelength-dependent secondary Dirac fermions (Yankowitz et al., 2012) in Graphene/h-BN moiré superlattices. With the knowledge from graphene, it was expected that moiré superlattice, twist-angle dependent physics, is also possible in TMDs heterostructure platform, which has been confirmed recently (Zhang et al., 2017a). The subject took momentum with the novel findings of unconventional superconductivity and correlation-driven insulating states at the magic angle (1.1°) in twisted bilayer graphene, depending on the electrostatic doping (Cao et al., 2018a, 2018b). IAX has been observed experimentally (Jin et al., 2019b) in WSe_2/WS_2 moiré heterostructure as per theoretical prediction (Wu et al., 2018a). Unlike intralayer moiré exciton, it is hard to get evidence for IEX in moiré HS by conventional optical measurements because of much lower absorption capability. Broad peaks with alternating left or right-handed circular polarization and sharp peaks having ~100 μeV linewidths with uniform circular polarization had been assigned to multiple interlayer resonances in moiré HS by different research groups (Alexeev et al., 2019; Jin et al., 2019a; Seyler et al., 2019; Tran et al., 2019). The past three years have witnessed a significant surge in theoretical and experimental research on correlated moiré systems to reveal exotic physical functionalities such as superconductor-Mott insulator transition in twisted bilayer graphene. Subsequently, a series of works have been enlisted with the discoveries of correlated Chern insulator and ferromagnetism in tri-layer graphene/hexagonal boron nitride system (Chen et al., 2020), topological superconductivity in $CrBr_3/NbSe_2$ (Kezilebieke et al., 2020), quantum phase transition from an antiferromagnetic state to a weak ferromagnetic state in strong-interaction regime (Tang et al., 2020), Mott insulator and Wigner crystals states in WSe_2/WS_2 (Regan et al., 2020), unconventional ferroelectricity in h-BN/bilayer graphene/hBN (Zheng et al., 2020), strip phases in WSe_2/WS_2 (Jin et al., 2021), correlated metallic as well as insulating states and topological magnetic state in twisted monolayer–bilayer graphene system (Chen et al., 2021), and correlated insulating states in WS_2/WSe_2 moiré lattice at fractional fillings (Huang et al., 2021).

Many exotic correlated quantum phases and topological states in 2D twisted-field have been explored. Many new functionalities such as multiferroics, topological insulators, and quantum spin liquids are expected to pave the way to exotic quantum devices. However, the progress in tuning HS geometry via changing the moiré atomic registry is limited to proof-of-concept studies, owing to samples prepared via mechanical transfer technique, which is a cumbersome process to control orientation and location of the flakes and suffers from interfacial contamination, scalability, and uncontrolled alignment. For lab-to-fab transition, large-scale CVD-grown samples are preferred. There should be a focus to develop a reliable CVD strategy that should be flexible to precisely control and manipulate twist angle *in situ*. However, the progress in this direction is not promising as most of the structures obtained either have the R-type (0°) stacking orientations or the H-type (60°) stacking orientations, as they are energetically favorable in the CVD growth process (Liu et al., 2014). Few strategies, including heterosite nucleation (Sun et al., 2021), temperature triggered misalignment (Omambac et al., 2019), metal-semiconductor stacking (Li et al., 2020a), epitaxial intercalation of graphene under hydrogen-terminated hBN template (Wang et al., 2021a), are recently reported that showed the potential of CVD to generate moiré phase. Still, stringent control on interlayer twist angle is challenging and needs to be encountered soon. Similar to twist angle, strain in vdW HS can open up a new possibility, 'Straintronics,' to manipulate electrical properties and light-matter interactions, largely unexplored. Novel CVD strategy with tunable twist angle in the weak, intermediate, and strong coupling regimes can open the way to observe correlated phases in a single experiment and move this field onestep closer to future quantum technology.

On the other hand, the presence of Moiré periodic-potential in incommensurate bilayer heterostructure is expected to give a unique pathway to tune diffusion, a critical parameter for transistor and photovoltaic devices. A small twist-angle results in a considerable moiré period that impedes diffusion (Choi et al., 2020; Yuan et al., 2020). Localization of IEX in vdW heterostructure leads to hosting an array of highly tunable quantum light emitters (Baek et al., 2020). In contrast, large twist-angle and small moiré periods prefer mobile excitons essential for the BEC phase of IEX. These innovative functionalities can unlock the way to (Twist + Opto)-excitonics by controlling, manipulating, and harnessing moiré excitonic states via device fabrication and pave the way to next-generation single-photon emitter arrays, semiconductor lasers, entangled photon sources, artificial excitonic crystals, and excitonic dielectric applications.

APPLICATIONS

Interest in 2D layered materials is growing day by day with ceaseless incorporation of new functionalities to their characteristics list, making them competent for next-generation electronics and optoelectronics applications. Thanks to their novel structural and electro-optical functionalities, 2D materials and their HSs are showing their potential promises and prospectus for a wide range of applications that includes energy harvesting, flexible devices, IoTs, transistors, photovoltaics, LEDs, photodetectors, sensors, exciton based switches, spintronics, and devices for quantum technology, which are summarized in Figure 5 (Dankert and Dash, 2017; Sahoo et al., 2019; Song et al., 2016; Wang et al., 2020; Wu et al., 2020; Wu et al., 2019a; Zhu et al., 2019). When we make HS of different semiconductor then they play an extensive role in tuning individuals functionalities and predicting new electronic devices and physics, which eventually will be helpful for industrial application. Work on complex ICs and logic gates has already been started using this 2D framework (Kim et al., 2021; Zhu et al., 2021). Not only limited to electronic or optoelectronic devices, but researchers are also continuously putting efforts into designing conventional or different structures with new combinations to explore the potential of the 2D framework in a new field and optimize the device's performance. (Guo et al., 2021; Kundu et al., 2021; Wang et al., 2021b) Most HS-based FET and TFET devices are drawn for electronics and low-power usages. First, the challenges associated with their performance are addressed, followed by possible pathways for optimization. FETs have been used as a building block for many electronic and optoelectronic applications.

A lot of progress in the structure and dimensionality of 2D hetero-assemble have been made until recently (Figure 6). Moreover, electronic devices for particular applications often require specific characteristics such as a high on/off ratio, high field-effect mobility, or low subthreshold swing (SS). Therefore, the reduction of FET size has been prioritized for device improvement. Still, problems such as leakage current (Gusev et al., 2001) and poor heat management (Assaderaghi et al., 2000) are detrimental to its performance. Therefore, the 2D material-based channel between source and drain became an alternative (Lee et al., 2021) to counter such problems, owing to their high on/off ratio and high mobility. (Braga et al., 2012; Liu et al., 2013; Pradhan et al., 2014; Wang et al., 2014). Graphene-based FETs were considered because of their excellent mobility ($\sim$350,000 cm^{2}V^{-1}s^{-1}) (Banszerus et al., 2015); however, their low on/off ratio (Chhowalla et al., 2016) and lack of bandgap hinder its use in FET applications. 2D black phosphorus (BP) (Li et al., 2014) showed an optimized value of on/off ratio and mobility. Recently InSe based FETs have shown even better results for both on/off ratio and mobility than BP (Jiang et al., 2019).

HSs are very much dependent on the type of materials taken, the substrate on which the HSs is made, and environmental condition. The electric properties also vary accordingly. For example, WSe$_2$/WS$_2$ VHS shows different rectification ratio (RR) values when the structures are made on different substrates that show the dependence of the FET parameter on the substrate (Chen et al., 2016; Li et al., 2016a). So, the choice of the substrate becomes crucial if one wants to get better performance. In MoS$_2$/WS$_2$ VHS configuration, the mobility is improved compared to pristine MoS$_2$-FET because of the charge transfer effect (Xu et al., 2021). When a WS$_2$/MoS$_2$/WS$_2$ tri-layer VHS is considered, the mobility is seen to improve even further because of the suppression of Coulomb scattering for such improvement (Xu et al., 2021).

Optimization of 2D HS FET devices is crucial for improving their performance. Gate tunability can be considered one of the optimization criteria for 2D electronic devices. This gate tunability in MoS$_2$ and single-walled carbon nanotubes HS helps the device to show an anti-ambipolar response (Jariwala et al., 2013). Another essential optimization issue for the 2D electronic device is the requirement of low resistance contacts. Several strategies were employed to reduce the contact resistances by reducing the Schottky barrier and reducing metal-induced gap states at the interfaces (Dankert et al., 2014; Das et al., 2013; Shen et al., 2021; Wang et al., 2019b). Utilizing 2D HS as active channel materials, graphene is used as electrodes with gate-tunable work function and helps in tuning the contact resistance (Lee et al., 2013; Yoon et al., 2013; Dankert and Dash, 2017). WSe$_2$ and graphene HS, though they do not form Ohmic contact, helps reduce Schottky barrier height and result in a low resistance (Das et al., 2014; Roy et al., 2014). It has also been seen that using h-BN as a dielectric layer helps curb the impurity scattering problem as they minimize the interface states (Hui et al., 2016; Pandey et al., 2018). The presence of intrinsic and extrinsic defects can also affect the device performance. Controlled tweaking of such defects has been shown to improve the characteristic properties of 2D devices. For example, tailoring sulfur vacancies improves mobility, high on/off ratio, and voltage gain in monolayer MoS$_2$. The underlying principle for better performance

is optimizing sulfur density leading to maximization of charge hopping probability. So, it is essential to consider such strategies to optimize the properties of HS using MoS_2 and other TMDs.

For low-power applications, MOSFETs have a fundamental problem of not reducing energy usage beyond the limit set by Boltzmann distribution, i.e., SS value capped at 60 mV/decade. To curb such energy usage issues, negative-capacitance FET (NC-FET) was introduced (Wang et al., 2019a). A flexible device composed of 2D MoS_2 and $CuInP_2S_6$ has been used as a logic inverter with a sub-60 mV dec^{-1} SS value. Reduction of power dissipation has always been the aim of increasing the efficiency of electronic devices for which TFETs can serve that purpose because of their low SS. 2D HS FET helps curb the low on-state current of 2D TFET. Conventional semiconductor-based TFETs have low SS value and low drive current, a shortcoming for high power computation (Gandhi et al., 2011). In this context, 2D TFETs have been made as an ideal choice owing to their low SS, high drive current, small tunneling distance, and efficient control over gate variability. However, in most 2D TFET (Fiori and Iannaccone, 2009), the off-state current is comparably high with respect to on-state current resulting in a low on-off ratio which can be addressed by using HSs as channel materials (Kim et al., 2020; Koo et al., 2018; Lan et al., 2016; Liu et al., 2017; Sarkar et al., 2015; Yan et al., 2017). 2D HS-based TFETs are devices made for ultra-low power substitutes and possess an ideal band structure for tunneling at different junction ends. It is also possible to regulate the on/off ratio by controlling different regions of heterojunction of TFET HS. Among others, black phosphorus (BP) and their HS have unique properties such as layer-dependent direct bandgap (Sun et al., 2017), suitable for 2D-TFET devices. Though multi-layered BP shows a good on/off ratio and SS value, the monolayer surpasses those values making it a strong contender for efficient TFET (Wu et al., 2019b). Recently, twisted black phosphorus homo-structure has been used to create a resonant tunneling diode with negative differential resistance, as usually in quantum-well structures (Srivastava et al., 2021). BP has been recently unveiled as a promising 2D semiconductor for spintronic devices using ferromagnetic source-drain contacts with the gate-tunable spin signal with nanosecond spin lifetimes (Avsar et al., 2017; Kamalakar et al., 2015).

Among mono-, bi-, and tri-layer phosphorene, the bilayer shows the highest on/off ratio (Ameen et al., 2016). Bilayer phosphorene is an ideal candidate for 2D-TFET because of its increased tunneling distance, reducing off current. In general, the constraint of ideal band-to-band tunneling of carriers is the Boltzmann limit of minimum SS, i.e., 60 mV per decade at 300 K. BP/MoS_2 HS has shown a good on/off ratio of about 10^5 with SS = 55 mV/dec (Liu et al., 2017). On the other hand, VHS of WSe_2 with $SnSe_2$ shows better performance with an SS value of 35 mV per decade and an on/off ratio of 10^5 compared to devices made from the WSe_2 layer (Oliva et al., 2020, p. 2). Though 2D-2D HS shows excellent SS and on/off values, 3D-2D HS showed better SS and on/off values (Kim et al., 2020; Sarkar et al., 2015). Ge/MoS_2 HS showed a very low SS value of about 3.9 mV/decade and a very high on/off ratio ideal for low power device applications (Sarkar et al., 2015). So different 2D-3D HS can be further explored for practical applications.

Most of the reported 2D-TFET devices are based on mechanically exfoliated samples, limiting further scalability progress. One of the possible ways to optimize SS value is by manipulating the device fabrication process and attaching different 2D materials with a particular bandgap of interest to maximize the result. Further efforts are needed to engineer the channel region in recent TFETs because of the lack of electrostatic controllability and defect in those particular regions. These properties are susceptible to device design, and hence much attention should be given during device fabrication. Low power consumption is another criterion for efficient device design. By regulating the supply voltage and the leakage current, it is possible to realize TFET with on-demand performance and low power consumption requirements. For both positive and negative input voltage, conduction is seen in TFET, making it challenging to design the circuitry. Low tunneling current and unbalanced current flowing in TFET devices are other reasons to be addressed to improve the circuit design. Most of these issues can be addressed using high electronic quality HSs with atomically precise and clean interfaces for high tunneling current and steep SS. Band-gap engineering is another way to be considered for designing ideal 2D-TFET devices. TFET handles drain-induced barrier lowering and hot charge carrier effect at smaller channel lengths effectively, for which it becomes a viable option for future applications. Another way to curb the power consumption could be using FET in negative differential resistance (NDR) mode using 2D HS devices (Lin et al., 2015; Nourbakhsh et al., 2016; Yan et al., 2015). In NDR, charge carrier injection can be carried out via tunneling from one band to another. Esaki-diodes made from $BP/SnSe_2$ HS (Yan et al., 2015) can be considered a promising NDR device. MoS_2/WSe_2 HS (Nourbakhsh et al., 2016) also shows a good NDR response. HS devices
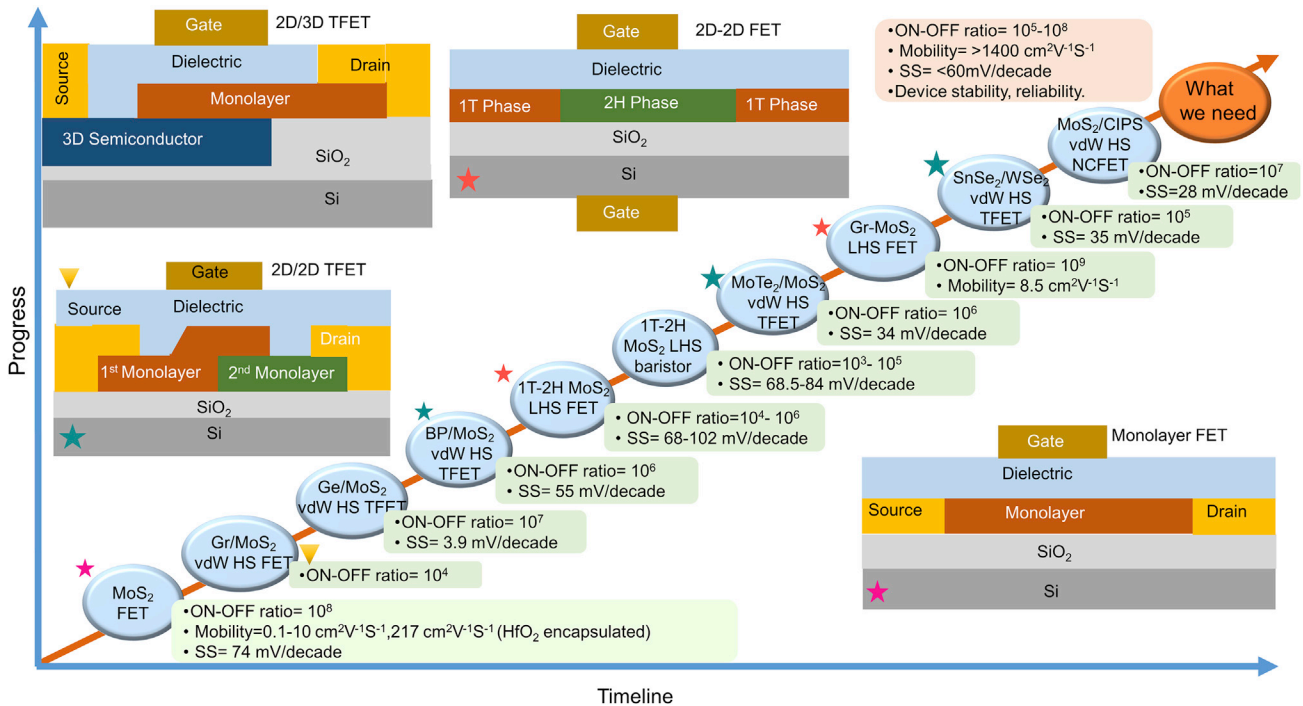
Figure 6. Progress-timeline graph

A progress-timeline graph depicting ON-OFF ratio, mobility, and SS values achieved to date via using FETs and TFETs of different heterostructures, with the inset schematic representing different structures with (a,c) TFET and (b.d) FET device configurations.

showing a good NDR response can be engineered to work at very low power. Such modification can be done by changing the way HS is stacked and the number of layers.

Apart from electronic applications, FET has been beneficial in exploring biological samples. For example, the usage of MoS_2 FETs as biosensors helped detect the proteins and hence analyzed the genetic information (Sarkar et al., 2014, p. 2). Furthermore, HS made of MoS_2 and graphene can be used as a nanocomposite of MoS_2, graphene, and horseradish peroxidase (HRP), which showed high sensitivity with high stability, selectivity, and reproducibility while using these materials as a biosensor (Song et al., 2014). All these properties are accounted for the excellent electron transport efficiency of MoS_2 and graphene HS in biological samples.

Recently, emerging phenomena have been observed in 2D material heterostructures providing a new platform beyond CMOS technology, as summarized in Figure 7. Significant effort has been dedicated to integrating logic with memory as a foundation for neuromorphic computing and logic-in-memory beyond von Neumann architecture (Christensen et al., 2021; LeCun et al., 2015). Several technologies have emerged, such as phase-change memory, resistive random access memory, and spintronic memory that simultaneously provides memory and logic units (Kaspar et al., 2021; Xia and Yang, 2019). The 2D materials and vdW heterostructures can enable unique neuromorphic responses with unprecedented control over their functionalities. Memristive functions were demonstrated utilizing various mechanisms, namely defect formation, migration, phase transitions, filament formation, and charge trapping in 2D semiconductors (Hus et al., 2021; Sangwan et al., 2015). This allows the realization of multi-terminal device design combining functionalities of the memristor and transistor, called memtransistor. Moreover, in memtransistors based on 2D semiconductor materials, the Schottky barrier is also found to be dynamically modulated by the type and concentration of defects and their bias-induced motion (Sangwan et al., 2018).

A recent report developed logic-in-memory devices based on floating-gate field-effect transistors with 2D semiconductors, in which logic operations can be directly performed using the memory elements(Migliato Marega et al., 2020). Furthermore, a twistronic approach was discovered to engineer ferroelectrics in van
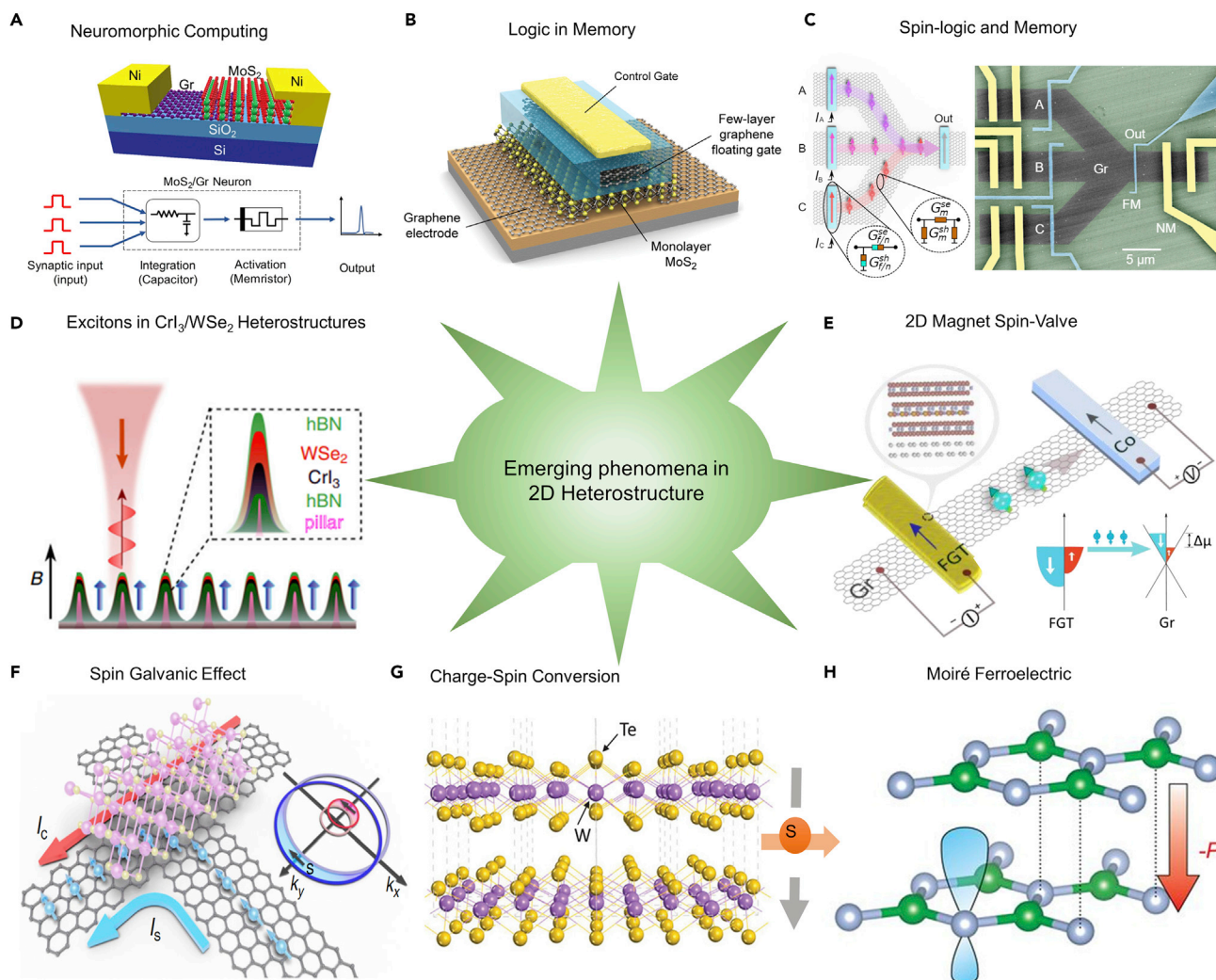
Figure 7. Emerging technologies in 2D materials and heterostructures

(A) Schematic of a MoS_2 memtransistor (Kalita et al., 2019). Copyright 2019, Springer Nature.

(B) Logic-in-memory in MoS_2 devices (Bertolazzi et al., 2013). Copyright 2013, American Chemical Society.

(C) Spin-logic with nonvolatile magnetic memory (Khokhriakov et al., 2021).

(D) Excitions on WSe_2 in heterostructure with a 2D magnet (Mukherjee et al., 2020). Copyright 2020, Springer Nature.

(E) Room temperature spin-valve with 2D magnets (Zhao et al., 2021).

(F) Spin galvanic effect in 2D materials heterostructure (Khokhriakov et al., 2020). Copyright 2020, Springer Nature.

(G) Charge-spin conversion in WTe_2 (Zhao et al., 2020). Copyright 2020, Wiley.

(H) Moiré ferroelectric with a twist angle between the hBN layers (Yasuda et al., 2021). Copyright 2020, AAAS

der Waals heterostructure of bilayer hBN (Vizner Stern et al., 2021; Yasuda et al., 2021). Twisting the 2D sheets by a small angle can change the switching dynamics because of the formation of moiré ferroelectricity with staggered polarization. This designer approaches for engineering vdW ferroelectrics in moiré superlattice can be explored in the future in 2D semiconductor materials to integrate nonvolatile memory and logic functions. Furthermore, all-spin-based computing combining logic and nonvolatile magnetic memory is promising for emerging information technologies. A recent experiment demonstrated a reprogrammable all-electrical multifunctional spin logic gate in a nanoelectronic device architecture utilizing graphene for spin communication, multiplexing, and nanomagnets for writing and reading information at room temperature (Khokhriakov et al., 2021). These findings highlight the potential of 2D materials for the development of all-electrical memtransistors and all-spin domain logic-in-memory architecture for energy-efficient neuromorphic computing.

The utilizations of TMDs are influencing a wide range of fields in condensed matter physics, from spintronics to realizing new quantum states of matter. Engineering TMDs in heterostructures with graphene is shown to yield a spin-transistor-like behavior (Dankert and Dash, 2017; Yan et al., 2016) with strong proximity induced charge-to-spin conversion effects such as spin Hall effect and Rashba-Edelsten effect up to room temperature (Benítez et al., 2020; Ghiasi et al., 2019). The proximity effects in van der Waals heterostructure of graphene with WSe_2 pave the way for engineering topological states and correlated quantum phases and are proposed to provide a tunable platform for more exotic device functionalities (Zollner et al., 2020). The research field is even emerging with the discovery of TMD semimetals, which also show a wide range of properties with Weyl semimetal phase (Soluyanov et al., 2015) in bulk and topological quantum spin Hall states (Wu et al., 2018b) in monolayer forms in WTe_2 with strong and unconventional charge-spin conversion (MacNeill et al., 2017; Zhao et al., 2020) effects. This large current-induced spin polarization can be possible in WTe_2 because of a reduced crystal symmetry combined with its large spin Berry curvature, spin-orbit interaction, and a novel spin-texture of the Weyl nodes and Fermi arc surface states. These advances open the door for developing spintronic memory (Dieny et al., 2020) and logic devices (Khokhriakov et al., 2021) with all-2D HSs, where the spin signal can be controlled by an electric field (Khokhriakov et al., 2020). Finally, the discovery of van der Waals magnets (Burch et al., 2018; Gong et al., 2017; Huang et al., 2017) opened a new paradigm for spintronic, superconducting, excitonic, and topological phenomena in all-2D heterostructures. Several emergent phenomena have been observed in TMDs in heterostructure with magnetic insulators, such as proximity induced magnetoluminescence, coupled spin-valley physics, valley excitonic Zeeman splitting (Seyler et al., 2018; Zhong et al., 2017, 2020). The investigations of magnetic proximity effects with superconductors (Kezilebieke et al., 2020) and graphene (Ghiasi et al., 2021; Karpiak et al., 2019) provide prospects of inducing topological superconducting effects and induced magnetism in van der Waals heterostructures. However, spintronic devices with vdW magnets are limited to cryogenic temperatures, inhibiting its broader practical applications. A recent report demonstrates room temperature spin-valve devices using vdW itinerant ferromagnet Fe_5GeTe_2 in heterostructures with graphene. These reports open new opportunities for all-2D heterostructure devices for various applications in electronics, spintronics, optoelectronics, and topological quantum devices.

OUTLOOK

2D materials and their HSs are emerging as prospective candidates to go beyond silicon-based electronics. With the uncovering of unconventional and fascinating 2D-physics and promising opto-electrical characteristics, they are maturing as a robust candidate for next-generation transparent, flexible, low-power optoelectronics and quantum technology. However, the progress in this direction is limited to mostly proof-of-concept studies owing to the lack of rational and scalable methods for the fabrication of HSs other than mechanical transfer techniques. To push the potential into real-world application, scalable synthesis of 2D HSs and hetero-integration of 2D devices are indispensable. Substantial efforts are made toward this direction, and CVD and MOCVD methods are claimed to be the most competent methods for commercialization. Still, several significant challenges need to be resolved, and a concrete understanding of growth kinetics is yet to be validated to bring 2D technology from academic research to real applications. Comprehensive future targets and growth mechanisms are systematically discussed in this article to draw attention to the challenging issues. Large-scale and electronic-grade quality 2D HSs with high controllability over interface width, layer number, doping, morphology, twist angle, and reliability via a universal growth strategy is the need of the hour to enter into the 2D paradigm. Apart from the synthesis issue, the environmental stability of devices is a big challenge that needs to be investigated seriously to witness extraordinary potential applications of 2D HSs at the ultimate thinness limits.

ACKNOWLEDGMENTS

AUTHOR CONTRIBUTIONS

All authors contributed to the discussion of contents, writing and revising the manuscript.

DECLARATION OF INTERESTS

The authors declare no competing interests.

REFERENCES

Alexeev, E.M., Ruiz-Tijerina, D.A., Danovich, M., Hamer, M.J., Terry, D.J., Nayak, P.K., Ahn, S., Pak, S., Lee, J., Sohn, J.I., et al. (2019). Resonantly hybridized excitons in moiré superlattices in van der Waals heterostructures. Nature 567, 81–86. https://doi.org/10.1038/s41586-019-0986-9.

Ameen, T.A., Ilatikhameneh, H., Klimeck, G., and Rahman, R. (2016). Few-layer phosphorene: an ideal 2D material for tunnel transistors. Sci. Rep. 6, 28515. https://doi.org/10.1038/srep28515.

Assaderaghi, F., Hsu, L.-C., and Allan, J. (2000). 73 Assignee, 10 (Armonk, N.Y.: International Business Machines Corporation).

Avsar, A., Tan, J.Y., Kurpas, M., Gmitra, M., Watanabe, K., Taniguchi, T., Fabian, J., and Özyilmaz, B. (2017). Gate-tunable black phosphorus spin valve with nanosecond spin lifetimes. Nat. Phys 13, 888–893. https://doi.org/10.1038/nphys4141.

Baek, H., Brotons-Gisbert, M., Koong, Z.X., Campbell, A., Rambach, M., Watanabe, K., Taniguchi, T., and Gerardot, B.D. (2020). Highly energy-tunable quantum light from moiré-trapped excitons. Sci. Adv. 6, eaba8526. https://doi.org/10.1126/sciadv.aba8526.

Banszerus, L., Schmitz, M., Engels, S., Dauber, J., Oellers, M., Haupt, F., Watanabe, K., Taniguchi, T., Beschoten, B., and Stampfer, C. (2015). Ultrahigh-mobility graphene devices from chemical vapor deposition on reusable copper. Sci. Adv. 1, e1500222. https://doi.org/10.1126/sciadv.1500222.

Benítez, L.A., Savero Torres, W., Sierra, J.F., Timmermans, M., Garcia, J.H., Roche, S., Costache, M.V., and Valenzuela, S.O. (2020). Tunable room-temperature spin galvanic and spin Hall effects in van der Waals heterostructures. Nat. Mater. 19, 170–175. https://doi.org/10.1038/s41563-019-0575-1.

Bertolazzi, S., Krasnozhon, D., and Kis, A. (2013). Nonvolatile memory cells based on MoS2/graphene heterostructures. ACS Nano 7, 3246–3252. https://doi.org/10.1021/nn3059136.

Berweger, S., Zhang, H., Sahoo, P.K., Kupp, B.M., Blackburn, J.L., Miller, E.M., Wallis, T.M., Voronine, D.V., Kabos, P., and Nanayakkara, S.U. (2020). Spatially resolved persistent photoconductivity in MoS2–WS2 lateral heterostructures. ACS Nano 14, 14080–14090. https://doi.org/10.1021/acsnano.0c06745.

Braga, D., Gutiérrez Lezama, I., Berger, H., and Morpurgo, A.F. (2012). Quantitative determination of the band gap of WS 2 with ambipolar ionic liquid-gated transistors. Nano Lett. 12, 5218–5223. https://doi.org/10.1021/nl302389d.

Briggs, N., Subramanian, S., Lin, Z., Li, X., Zhang, X., Zhang, K., Xiao, K., Geohegan, D., Wallace, R., Chen, L.-Q., et al. (2019). A roadmap for electronic grade 2D materials. 2D Mater. 6, 022001. https://doi.org/10.1088/2053-1583/aaf836.

Britnell, L., Ribeiro, R.M., Eckmann, A., Jalil, R., Belle, B.D., Mishchenko, A., Kim, Y.-J., Gorbachev, R.V., Georgiou, T., Morozov, S.V., et al. (2013). Strong light-matter interactions in heterostructures of atomically thin films. Science 340, 1311–1314. https://doi.org/10.1126/science.1235547.

Burch, K.S., Mandrus, D., and Park, J.-G. (2018). Magnetism in two-dimensional van der Waals materials. Nature 563, 47–52. https://doi.org/10.1038/s41586-018-0631-z.

Calado, V.E., Schneider, G.F., Theulings, A.M.M.G., Dekker, C., and Vandersypen, L.M.K. (2012). Formation and control of wrinkles in graphene by the wedging transfer method. Appl. Phys. Lett. 101, 103116. https://doi.org/10.1063/1.4751982.

Cao, L., Cao, L., Zhong, J., Zhong, J., Yu, J., Yu, J., Zeng, C., Ding, J., Cong, C., Yue, X., et al. (2020). Valley-polarized local excitons in WSe2/WS2 vertical heterostructures. Opt. Express, OE 28, 22135–22143. https://doi.org/10.1364/OE.399142.

Cao, Y., Fatemi, V., Demir, A., Fang, S., Tomarken, S.L., Luo, J.Y., Sanchez-Yamagishi, J.D., Watanabe, K., Taniguchi, T., Kaxiras, E., et al. (2018a). Correlated insulator behaviour at half-filling in magic-angle graphene superlattices. Nature 556, 80–84. https://doi.org/10.1038/nature26154.

Cao, Y., Fatemi, V., Fang, S., Watanabe, K., Taniguchi, T., Kaxiras, E., and Jarillo-Herrero, P. (2018b). Unconventional superconductivity in magic-angle graphene superlattices. Nature 556, 43–50. https://doi.org/10.1038/nature26160.

Castellanos-Gomez, A., Buscema, M., Molenaar, R., Singh, V., Janssen, L., van derZant, H.S.J., and Steele, G.A. (2014). Deterministic transfer of two-dimensional materials by all-dry viscoelastic stamping. 2D Mater. 1, 011002. https://doi.org/10.1088/2053-1583/1/1/011002.

Chaves, A., Azadani, J.G., Alsalman, H., da Costa, D.R., Frisenda, R., Chaves, A.J., Song, S.H., Kim, Y.D., He, D., Zhou, J., et al. (2020). Bandgap engineering of two-dimensional semiconductor materials. Npj 2D Mater. Appl. 4, 1–21. https://doi.org/10.1038/s41699-020-00162-4.

Chen, G., Sharpe, A.L., Fox, E.J., Zhang, Y.-H., Wang, S., Jiang, L., Lyu, B., Li, H., Watanabe, K., Taniguchi, T., et al. (2020). Tunable correlated Chern insulator and ferromagnetism in a moiré superlattice. Nature 579, 56–61. https://doi.org/10.1038/s41586-020-2049-7.

Chen, J., Zhou, W., Tang, W., Tian, B., Zhao, X., Xu, H., Liu, Y., Geng, D., Tan, S.J.R., Fu, W., and Loh, K.P. (2016). Lateral epitaxy of atomically sharp WSe 2/WS 2 heterojunctions on silicon dioxide substrates. Chem. Mater. 28, 7194–7197. https://doi.org/10.1021/acs.chemmater.6b03639.

Chen, K., Wan, X., Xie, W., Wen, J., Kang, Z., Zeng, X., Chen, H., and Xu, J. (2015). Lateral built-in potential of monolayer MoS2–WS2 in-plane heterostructures by a shortcut growth strategy. Adv. Mater. 27, 6431–6437. https://doi.org/10.1002/adma.201502375.

Chen, S., He, M., Zhang, Y.-H., Hsieh, V., Fei, Z., Watanabe, K., Taniguchi, T., Cobden, D.H., Xu, X., Dean, C.R., and Yankowitz, M. (2021). Electrically tunable correlated and topological states in twisted monolayer–bilayer graphene. Nat. Phys. 17, 374–380. https://doi.org/10.1038/s41567-020-01062-6.

Chen, T., Ding, D., Shi, J., Wang, G., Kou, L., Zheng, X., Ren, X., Liu, X., Jin, C., Zhong, J., and Hao, G. (2019). Lateral and vertical MoSe2–MoS2 heterostructures via epitaxial growth: triggered by high-temperature annealing and precursor concentration. J. Phys. Chem. Lett. 10, 5027–5035. https://doi.org/10.1021/acs.jpclett.9b01961.

Chernikov, A., Berkelbach, T.C., Hill, H.M., Rigosi, A., Li, Y., Aslan, O.B., Reichman, D.R., Hybertsen, M.S., and Heinz, T.F. (2014). Exciton binding energy and nonhydrogenic Rydberg series in monolayer WS2. Phys. Rev. Lett. 113, 076802. https://doi.org/10.1103/PhysRevLett.113.076802.

Chhowalla, M., Jena, D., and Zhang, H. (2016). Two-dimensional semiconductors for transistors. Nat. Rev. Mater. 1, 16052. https://doi.org/10.1038/natrevmats.2016.52.

Chiu, K.-C., Huang, K.-H., Chen, C.-A., Lai, Y.-Y., Zhang, X.-Q., Lin, E.-C., Chuang, M.-H., Wu, J.-M., and Lee, Y.-H. (2018). Synthesis of in-plane artificial lattices of monolayer multijunctions. Adv. Mater. 30, 1704796. https://doi.org/10.1002/adma.201704796.

Cho, B., Yoon, J., Lim, S.K., Kim, A.R., Kim, D.-H., Park, S.-G., Kwon, J.-D., Lee, Y.-J., Lee, K.-H., Lee, B.H., et al. (2015). Chemical sensing of 2D graphene/MoS2 heterostructure device. ACS Appl. Mater. Inter. 7, 16775–16780. https://doi.org/10.1021/acsami.5b04541.

Choi, J., Hsu, W.-T., Lu, L.-S., Sun, L., Cheng, H.-Y., Lee, M.-H., Quan, J., Tran, K., Wang, C.-Y., Staab, M., et al. (2020). Moiré potential impedes interlayer exciton diffusion in van der Waals heterostructures. Sci. Adv. 6, eaba8866. https://doi.org/10.1126/sciadv.aba8866.

Christensen, D.V., Dittmann, R., Linares-Barranco, B., Sebastian, A., Gallo, M.L., Redaelli, A., Slesazeck, S., Mikolajick, T., Spiga, S., Menzel, S., et al. (2021). 2021 roadmap on neuromorphic computing and engineering. https://arxiv.org/abs/2105.05956.

Ciarrocchi, A., Unuchek, D., Avsar, A., Watanabe, K., Taniguchi, T., and Kis, A. (2019). Polarization switching and electrical control of interlayer excitons in two-dimensional van der Waals heterostructures. Nat. Photon 13, 131–136. https://doi.org/10.1038/s41566-018-0325-y.

Dankert, A., and Dash, S.P. (2017). Electrical gate control of spin current in van der Waals heterostructures at room temperature. Nat. Commun. 8, 16093. https://doi.org/10.1038/ncomms16093.

Dankert, A., Karpiak, B., and Dash, S.P. (2017). Hall sensors batch-fabricated on all-CVD h-BN/graphene/h-BN heterostructures. Sci. Rep. 7, 15231. https://doi.org/10.1038/s41598-017-12277-8.

Dankert, A., Langouche, L., Kamalakar, M.V., and Dash, S.P. (2014). High-performance molybdenum disulfide field-effect transistors with spin tunnel contacts. ACS Nano 8, 476–482. https://doi.org/10.1021/nn404961e.

Das, S., Chen, H.-Y., Penumatcha, A.V., and Appenzeller, J. (2013). High performance multilayer MoS2 transistors with scandium contacts. Nano Lett. *13*, 100–105. https://doi.org/10.1021/nl303583v.

Das, S., Gulotty, R., Sumant, A.V., and Roelofs, A. (2014). All two-dimensional, flexible, transparent, and thinnest thin film transistor. Nano Lett. *14*, 2861–2866. https://doi.org/10.1021/nl5009037.

Dean, C.R., Wang, L., Maher, P., Forsythe, C., Ghahari, F., Gao, Y., Katoch, J., Ishigami, M., Moon, P., Koshino, M., et al. (2013). Hofstadter's butterfly and the fractal quantum Hall effect in moiré superlattices. Nature *497*, 598–602. https://doi.org/10.1038/nature12186.

Dean, C.R., Young, A.F., Meric, I., Lee, C., Wang, L., Sorgenfrei, S., Watanabe, K., Taniguchi, T., Kim, P., Shepard, K.L., and Hone, J. (2010). Boron nitride substrates for high-quality graphene electronics. Nat. Nanotech *5*, 722–726. https://doi.org/10.1038/nnano.2010.172.

Dieny, B., Prejbeanu, I.L., Garello, K., Gambardella, P., Freitas, P., Lehndorff, R., Raberg, W., Ebels, U., Demokritov, S.O., Akerman, J., et al. (2020). Opportunities and challenges for spintronics in the microelectronics industry. Nat.Electron *3*, 446–459. https://doi.org/10.1038/s41928-020-0461-5.

Du, X., Skachko, I., Barker, A., and Andrei, E.Y. (2008). Approaching ballistic transport in suspended graphene. Nat. Nanotech *3*, 491–495. https://doi.org/10.1038/nnano.2008.199.

Duan, X., Wang, C., Shaw, J.C., Cheng, R., Chen, Y., Li, H., Wu, X., Tang, Y., Zhang, Q., Pan, A., et al. (2014). Lateral epitaxial growth of two-dimensional layered semiconductor heterojunctions. Nat. Nanotech *9*, 1024–1030. https://doi.org/10.1038/nnano.2014.222.

Fiori, G., and Iannaccone, G. (2009). Ultralow-voltage bilayer graphene tunnel FET. IEEE Electron Device Lett. *30*, 1096–1098. https://doi.org/10.1109/LED.2009.2028248.

Fogler, M.M., Butov, L.V., and Novoselov, K.S. (2014). High-temperature superfluidity with indirect excitons in van der Waals heterostructures. Nat. Commun. *5*, 4555. https://doi.org/10.1038/ncomms5555.

Fu, Q., Wang, X., Zhou, J., Xia, J., Zeng, Q., Lv, D., Zhu, C., Wang, X., Shen, Y., Li, X., et al. (2018). One-step synthesis of metal/semiconductor heterostructure NbS2/MoS2. Chem. Mater. *30*, 4001–4007. https://doi.org/10.1021/acs.chemmater.7b05117.

Gandhi, R., Chen, Z., Singh, N., Banerjee, K., and Lee, S. (2011). Vertical Si-nanowire n-Type tunneling FETs with low subthreshold swing (≤ 50 mV/decade) at room temperature. IEEE Electron Device Lett. *32*, 437–439. https://doi.org/10.1109/LED.2011.2106757.

Ghiasi, T.S., Kaverzin, A.A., Blah, P.J., and van Wees, B.J. (2019). Charge-to-Spin conversion by the Rashba–Edelstein effect in two-dimensional van der Waals heterostructures up to room temperature. Nano Lett. *19*, 5959–5966. https://doi.org/10.1021/acs.nanolett.9b01611.

Ghiasi, T.S., Kaverzin, A.A., Dismukes, A.H., de Wal, D.K., Roy, X., and van Wees, B.J. (2021).

Electrical and thermal generation of spin currents by magnetic bilayer graphene. Nat. Nanotechnol. *16*, 788–794. https://doi.org/10.1038/s41565-021-00887-3.

Gong, C., Li, L., Li, Z., Ji, H., Stern, A., Xia, Y., Cao, T., Bao, W., Wang, C., Wang, Y., et al. (2017). Discovery of intrinsic ferromagnetism in two-dimensional van der Waals crystals. Nature *546*, 265–269. https://doi.org/10.1038/nature22060.

Gong, Y., Lei, S., Ye, G., Li, B., He, Y., Keyshar, K., Zhang, X., Wang, Q., Lou, J., Liu, Z., et al. (2015). Two-step growth of two-dimensional WSe2/MoSe2 heterostructures. Nano Lett. *15*, 6135–6141. https://doi.org/10.1021/acs.nanolett.5b02423.

Gong, Y., Lin, J., Wang, X., Shi, G., Lei, S., Lin, Z., Zou, X., Ye, G., Vajtai, R., Yakobson, B.I., et al. (2014). Vertical and in-plane heterostructures from WS 2/MoS 2 monolayers. Nat. Mater *13*, 1135–1142. https://doi.org/10.1038/nmat4091.

Guo, H.-W., Hu, Z., Liu, Z.-B., and Tian, J.-G. (2021). Stacking of 2D materials. Adv. Funct. Mater. *31*, 2007810. https://doi.org/10.1002/adfm.202007810.

Gusev, E.P., Buchanan, D.A., Cartier, E., Kumar, A., DiMaria, D., Guha, S., Callegari, A., Zafar, S., Jamison, P.C., Neumayer, D.A., et al. (2001). Ultrathin high-K gate stacks for advanced CMOS devices. In International Electron Devices Meeting. Technical Digest (Cat. No. 01CH37224). Presented at the International Electron Devices Meeting (Technical Digest, IEEE). https://doi.org/10.1109/IEDM.2001.979537.

Heo, H., Sung, J.H., Jin, G., Ahn, J.-H., Kim, K., Lee, M.-J., Cha, S., Choi, H., and Jo, M.-H. (2015). Rotation-misfit-free heteroepitaxial stacking and stitching growth of hexagonal transition-metal dichalcogenide monolayers by nucleation kinetics controls. Adv. Mater. *27*, 3803–3810. https://doi.org/10.1002/adma.201500846.

Hong, X., Kim, J., Shi, S.-F., Zhang, Y., Jin, C., Sun, Y., Tongay, S., Wu, J., Zhang, Y., and Wang, F. (2014). Ultrafast charge transfer in atomically thin MoS 2/WS 2 heterostructures. Nat. Nanotech *9*, 682–686. https://doi.org/10.1038/nnano.2014.167.

Huang, B., Clark, G., Navarro-Moratalla, E., Klein, D.R., Cheng, R., Seyler, K.L., Zhong, D., Schmidgall, E., McGuire, M.A., Cobden, D.H., et al. (2017). Layer-dependent ferromagnetism in a van der Waals crystal down to the monolayer limit. Nature *546*, 270–273. https://doi.org/10.1038/nature22391.

Huang, C., Wu, S., Sanchez, A.M., Peters, J.J.P., Beanland, R., Ross, J.S., Rivera, P., Yao, W., Cobden, D.H., and Xu, X. (2014). Lateral heterojunctions within monolayer MoSe 2 –WSe 2 semiconductors. Nat. Mater *13*, 1096–1101. https://doi.org/10.1038/nmat4064.

Huang, X., Wang, T., Miao, S., Wang, C., Li, Z., Lian, Z., Taniguchi, T., Watanabe, K., Okamoto, S., Xiao, D., et al. (2021). Correlated insulating states at fractional fillings of the WS2/WSe2 moiré lattice. Nat. Phys. *17*, 715–719. https://doi.org/10.1038/s41567-021-01171-w.

Huang, Y., Pan, Y.-H., Yang, R., Bao, L.-H., Meng, L., Luo, H.-L., Cai, Y.-Q., Liu, G.-D., Zhao, W.-J., Zhou, Z., et al. (2020). Universal mechanical

exfoliation of large-area 2D crystals. Nat. Commun. *11*, 2453. https://doi.org/10.1038/s41467-020-16266-w.

Hui, F., Pan, C., Shi, Y., Ji, Y., Grustan-Gutierrez, E., and Lanza, M. (2016). On the use of two dimensional hexagonal boron nitride as dielectric. Microelectronic Eng. *163*, 119–133. https://doi.org/10.1016/j.mee.2016.06.015.

Hus, S.M., Ge, R., Chen, P.-A., Liang, L., Donnelly, G.E., Ko, W., Huang, F., Chiang, M.-H., Li, A.-P., and Akinwande, D. (2021). Observation of single-defect memristor in an MoS2 atomic sheet. Nat. Nanotechnol. *16*, 58–62. https://doi.org/10.1038/s41565-020-00789-w.

Jariwala, D., Sangwan, V.K., Wu, C.-C., Prabhumirashi, P.L., Geier, M.L., Marks, T.J., Lauhon, L.J., and Hersam, M.C. (2013). Gate-tunable carbon nanotube-MoS2 heterojunction p-n diode. Proc. Natl. Acad. Sci. U S A *110*, 18076–18080. https://doi.org/10.1073/pnas.1317226110.

Jiang, C., Xu, W., Rasmita, A., Huang, Z., Li, K., Xiong, Q., and Gao, W. (2018). Microsecond dark-exciton valley polarization memory in two-dimensional heterostructures. Nat. Commun. *9*, 753. https://doi.org/10.1038/s41467-018-03174-3.

Jiang, J., Li, J., Li, Y., Duan, J., Li, L., Tian, Y., Zong, Z., Zheng, H., Feng, X., Li, Q., et al. (2019). Stable InSe transistors with high-field effect mobility for reliable nerve signal sensing. Npj 2D Mater. Appl. *3*, 1–8. https://doi.org/10.1038/s41699-019-0110-x.

Jin, C., Regan, E.C., Wang, D., Iqbal Bakti Utama, M., Yang, C.-S., Cain, J., Qin, Y., Shen, Y., Zheng, Z., Watanabe, K., et al. (2019a). Identification of spin, valley and moiré quasi-angular momentum of interlayer excitons. Nat. Phys. *15*, 1140–1144. https://doi.org/10.1038/s41567-019-0631-4.

Jin, C., Regan, E.C., Yan, A., Iqbal Bakti Utama, M., Wang, D., Zhao, S., Qin, Y., Yang, S., Zheng, Z., Shi, S., et al. (2019b). Observation of moiré excitons in WSe 2/WS 2 heterostructure superlattices. Nature *567*, 76–80. https://doi.org/10.1038/s41586-019-0976-y.

Jin, C., Tao, Z., Li, T., Xu, Y., Tang, Y., Zhu, J., Liu, S., Watanabe, K., Taniguchi, T., Hone, J.C., et al. (2021). Stripe phases in WSe2/WS2 moiré superlattices. Nat. Mater. *20*, 940–944. https://doi.org/10.1038/s41563-021-00959-8.

Kalita, H., Krishnaprasad, A., Choudhary, N., Das, S., Dev, D., Ding, Y., Tetard, L., Chung, H.-S., Jung, Y., and Roy, T. (2019). Artificial neuron using vertical MoS2/graphene threshold switching memristors. Sci. Rep. *9*, 53. https://doi.org/10.1038/s41598-018-35828-z.

Kamalakar, M.V., Dankert, A., Kelly, P.J., and Dash, S.P. (2016). Inversion of spin signal and spin filtering in Ferromagnet|Hexagonal boron nitride-graphene van der Waals heterostructures. Sci. Rep. *6*, 21168. https://doi.org/10.1038/srep21168.

Kamalakar, M.V., Madhushankar, B.N., Dankert, A., and Dash, S.P. (2015). Low Schottky barrier black phosphorus field-effect devices with ferromagnetic tunnel contacts. Small *11*, 2209–2216. https://doi.org/10.1002/smll.201402900.

Karpiak, B., Cummings, A.W., Zollner, K., Vila, M., Khokhriakov, D., Hoque, A.M., Dankert, A., Svedlindh, P., Fabian, J., Roche, S., and Dash, S.P. (2019). Magnetic proximity in a van der Waals heterostructure of magnetic insulator and graphene. 2D Mater. 7, 015026. https://doi.org/10.1088/2053-1583/ab5915.

Kaspar, C., Ravoo, B.J., van der Wiel, W.G., Wegner, S.V., and Pernice, W.H.P. (2021). The rise of intelligent matter. Nature 594, 345–355. https://doi.org/10.1038/s41586-021-03453-y.

Kezilebieke, S., Huda, M.N., Vaňo, V., Aapro, M., Ganguli, S.C., Silveira, O.J., Głodzik, S., Foster, A.S., Ojanen, T., and Liljeroth, P. (2020). Topological superconductivity in a van der Waals heterostructure. Nature 588, 424–428. https://doi.org/10.1038/s41586-020-2989-y.

Khokhriakov, D., Hoque, A.M., Karpiak, B., and Dash, S.P. (2020). Gate-tunable spin-galvanic effect in graphene-topological insulator van der Waals heterostructures at room temperature. Nat. Commun. 11, 3657. https://doi.org/10.1038/s41467-020-17481-1.

Khokhriakov, D., Sayed, S., Hoque, A.M., Karpiak, B., Zhao, B., Datta, S., and Dash, S.P. (2021). Multifunctional spin logic gates in graphene spin circuits. https://arxiv.org/abs/2108.12259.

Kim, J., Jin, C., Chen, B., Cai, H., Zhao, T., Lee, P., Kahn, S., Watanabe, K., Taniguchi, T., Tongay, S., et al. (2017). Observation of ultralong valley lifetime in WSe2/MoS2 heterostructures. Sci. Adv. 3, e1700518. https://doi.org/10.1126/sciadv.1700518.

Kim, S., Myeong, G., Shin, W., Lim, H., Kim, B., Jin, T., Chang, S., Watanabe, K., Taniguchi, T., and Cho, S. (2020). Thickness-controlled black phosphorus tunnel field-effect transistor for low-power switches. Nat. Nanotechnol. 15, 203–206. https://doi.org/10.1038/s41565-019-0623-7.

Kim, T.W., Ra, H.S., Ahn, J., Jang, J., Taniguchi, T., Watanabe, K., Shim, J.W., Lee, Y.T., and Hwang, D.K. (2021). Frequency doubler and universal logic gate based on two-dimensional transition metal dichalcogenide transistors with low power consumption. ACS Appl. Mater. Inter. 13, 7470–7475. https://doi.org/10.1021/acsami.0c21222.

Kobayashi, Y., Yoshida, S., Maruyama, M., Mogi, H., Murase, K., Maniwa, Y., Takeuchi, O., Okada, S., Shigekawa, H., and Miyata, Y. (2019). Continuous heteroepitaxy of two-dimensional heterostructures based on layered chalcogenides. ACS Nano 13, 7527–7535. https://doi.org/10.1021/acsnano.8b07991.

Koo, B., Shin, G.H., Park, H., Kim, H., and Choi, S.-Y. (2018). Vertical-tunneling field-effect transistor based on MoTe2/MoS2 2D–2D heterojunction. J. Phys. D: Appl. Phys. 51, 475101. https://doi.org/10.1088/1361-6463/aae2a7.

Kundu, B., Mohanty, P., Kumar, P., Nayak, B., Mahato, B., Ranjan, P., Chakraborty, S.K., Sahoo, S., and Sahoo, P.K. (2021). Synthesis of lateral heterostructure of 2D materials for optoelectronic devices: challenges and opportunities. Emergent Mater. 4, 923–949. https://doi.org/10.1007/s42247-021-00219-0.

Lan, Y.-W., Torres, C.M., Tsai, S.-H., Zhu, X., Shi, Y., Li, M.-Y., Li, L.-J., Yeh, W.-K., and Wang, K.L. (2016). Atomic-monolayer MoS2 band-to-band tunneling field-effect transistor. Small 12, 5676–5683. https://doi.org/10.1002/smll.201601310.

LeCun, Y., Bengio, Y., and Hinton, G. (2015). Deep learning. Nature 521, 436–444. https://doi.org/10.1038/nature14539.

Lee, G.-H., Yu, Y.-J., Cui, X., Petrone, N., Lee, C.-H., Choi, M.S., Lee, D.-Y., Lee, C., Yoo, W.J., Watanabe, K., et al. (2013). Flexible and transparent MoS2 field-effect transistors on hexagonal boron nitride-graphene heterostructures. ACS Nano 7, 7931–7936. https://doi.org/10.1021/nn402954e.

Lee, I., Kang, W.T., Kim, J.E., Kim, Y.R., Won, U.Y., Lee, Y.H., and Yu, W.J. (2020). Photoinduced tuning of Schottky barrier height in graphene/MoS2 heterojunction for ultrahigh performance short channel phototransistor. ACS Nano 14, 7574–7580. https://doi.org/10.1021/acsnano.0c03425.

Lee, J., Pak, S., Lee, Y.-W., Park, Y., Jang, A.-R., Hong, J., Cho, Y., Hou, B., Lee, S., Jeong, H.Y., et al. (2019). Direct epitaxial synthesis of selective two-dimensional lateral heterostructures. ACS Nano 13, 13047–13055. https://doi.org/10.1021/acsnano.9b05722.

Lee, J.-H., Shin, D.H., Yang, H., Jeong, N.B., Park, D.-H., Watanabe, K., Taniguchi, T., Kim, E., Lee, S.W., Jhang, S.H., et al. (2021). Semiconductor-less vertical transistor with ION/IOFF of 106. Nat. Commun. 12, 1000. https://doi.org/10.1038/s41467-021-21138-y.

Li, H., Li, P., Huang, J.-K., Li, M.-Y., Yang, C.-W., Shi, Y., Zhang, X.-X., and Li, L.-J. (2016a). Laterally stitched heterostructures of transition metal dichalcogenide: chemical vapor deposition growth on lithographically patterned area. ACS Nano 10, 10516–10523. https://doi.org/10.1021/acsnano.6b06496.

Li, J., Yang, X., Liu, Y., Huang, B., Wu, R., Zhang, Z., Zhao, B., Ma, H., Dang, W., Wei, Z., et al. (2020a). General synthesis of two-dimensional van der Waals heterostructure arrays. Nature 579, 368–374. https://doi.org/10.1038/s41586-020-2098-y.

Li, L., Yu, Y., Ye, G.J., Ge, Q., Ou, X., Wu, H., Feng, D., Chen, X.H., and Zhang, Y. (2014). Black phosphorus field-effect transistors. Nat. Nanotech 9, 372–377. https://doi.org/10.1038/nnano.2014.35.

Li, M.-Y., Shi, Y., Cheng, C.-C., Lu, L.-S., Lin, Y.-C., Tang, H.-L., Tsai, M.-L., Chu, C.-W., Wei, K.-H., He, J.-H., et al. (2015). Epitaxial growth of a monolayer WSe2-MoS2 lateral p-n junction with an atomically sharp interface. Science 349, 524–528. https://doi.org/10.1126/science.aab4097.

Li, W., Lu, X., Dubey, S., Devenica, L., and Srivastava, A. (2020b). Dipolar interactions between localized interlayer excitons in van der Waals heterostructures. Nat. Mater. 19, 624–629. https://doi.org/10.1038/s41563-020-0661-4.

Li, X., Lin, M.-W., Lin, J., Huang, B., Puretzky, A.A., Ma, C., Wang, K., Zhou, W., Pantelides, S.T., Chi, M., et al. (2016b). Two-dimensional GaSe/MoSe2 misfit bilayer heterojunctions by van der Waals epitaxy. Sci. Adv. 2, e1501882. https://doi.org/10.1126/sciadv.1501882.

Liang, S.-J., Liu, B., Hu, W., Zhou, K., and Ang, L.K. (2017). Thermionic energy conversion based on graphene van der Waals heterostructures. Sci. Rep. 7, 46211. https://doi.org/10.1038/srep46211.

Lin, Y.-C., Ghosh, R.K., Addou, R., Lu, N., Eichfeld, S.M., Zhu, H., Li, M.-Y., Peng, X., Kim, M.J., Li, L.-J., et al. (2015). Atomically thin resonant tunnel diodes built from synthetic van der Waals heterostructures. Nat. Commun. 6, 7311. https://doi.org/10.1038/ncomms8311.

Liu, D., Hong, J., Li, X., Zhou, X., Jin, B., Cui, Q., Chen, J., Feng, Q., Xu, C., Zhai, T., et al. (2020). Synthesis of 2H-1T′ WS2-ReS2 heterophase structures with atomically sharp interface via hydrogen-triggered one-pot growth. Adv. Funct. Mater. 30, 1–11. https://doi.org/10.1002/adfm.201910169.

Liu, H., Li, D., Ma, C., Zhang, X., Sun, X., Zhu, C., Zheng, B., Zou, Z., Luo, Z., Zhu, X., et al. (2019). Van der Waals epitaxial growth of vertically stacked Sb2Te3/MoS2 p–n heterojunctions for high performance optoelectronics. Nano Energy 59, 66–74. https://doi.org/10.1016/j.nanoen.2019.02.032.

Liu, K., Zhang, L., Cao, T., Jin, C., Qiu, D., Zhou, Q., Zettl, A., Yang, P., Louie, S.G., and Wang, F. (2014). Evolution of interlayer coupling in twisted molybdenum disulfide bilayers. Nat. Commun. 5, 4966. https://doi.org/10.1038/ncomms5966.

Liu, W., Kang, J., Sarkar, D., Khatami, Y., Jena, D., and Banerjee, K. (2013). Role of metal contacts in designing high-performance monolayer n-type WSe2 field effect transistors. Nano Lett. 13, 1983–1990. https://doi.org/10.1021/nl304777e.

Liu, X., Qu, D., Li, H.-M., Moon, I., Ahmed, F., Kim, C., Lee, M., Choi, Y., Cho, J.H., Hone, J.C., and Yoo, W.J. (2017). Modulation of quantum tunneling via a vertical two-dimensional black phosphorus and molybdenum disulfide p–n junction. ACS Nano 11, 9143–9150. https://doi.org/10.1021/acsnano.7b03994.

Liu, Y., Duan, X., Shin, H.-J., Park, S., Huang, Y., and Duan, X. (2021). Promises and prospects of two-dimensional transistors. Nature 591, 43–53. https://doi.org/10.1038/s41586-021-03339-z.

Ma, H., Huang, K., Wu, R., Zhang, Z., Li, J., Zhao, B., Dai, C., Huang, Z., Zhang, H., Yang, X., et al. (2021). In-plane epitaxial growth of 2D CoSe-WSe2 metal-semiconductor lateral heterostructures with improved WSe2 transistors performance. InfoMat 3, 222–228. https://doi.org/10.1002/inf2.12157.

Ma, Y., Ajayan, P.M., Yang, S., and Gong, Y. (2018). Recent advances in synthesis and applications of 2D junctions. Small 14, 1801606. https://doi.org/10.1002/smll.201801606.

MacNeill, D., Stiehl, G.M., Guimaraes, M.H.D., Buhrman, R.A., Park, J., and Ralph, D.C. (2017). Control of spin–orbit torques through crystal symmetry in WTe2/ferromagnet bilayers. Nat. Phys 13, 300–305. https://doi.org/10.1038/nphys3933.

Mai, C., Barrette, A., Yu, Y., Semenov, Y.G., Kim, K.W., Cao, L., and Gundogdu, K. (2014). Many-body effects in valleytronics: direct measurement of valley lifetimes in single-layer MoS2. Nano Lett. 14, 202–206. https://doi.org/10.1021/nl403742j.

Mak, K.F., Lee, C., Hone, J., Shan, J., and Heinz, T.F. (2010). Atomically thin MoS_2: a new direct-gap semiconductor. Phys. Rev. Lett. 105, 136805. https://doi.org/10.1103/PhysRevLett.105.136805.

Mak, K.F., and Shan, J. (2016). Photonics and optoelectronics of 2D semiconductor transition metal dichalcogenides. Nat. Photon 10, 216–226. https://doi.org/10.1038/nphoton.2015.282.

Maragkou, M. (2015). The dark exciton as a qubit. Nat. Mater 14, 260. https://doi.org/10.1038/nmat4243.

Migliato Marega, G., Zhao, Y., Avsar, A., Wang, Z., Tripathi, M., Radenovic, A., and Kis, A. (2020). Logic-in-memory based on an atomically thin semiconductor. Nature 587, 72–77. https://doi.org/10.1038/s41586-020-2861-0.

Miller, B., Steinhoff, A., Pano, B., Klein, J., Jahnke, F., Holleitner, A., and Wurstbauer, U. (2017). Long-lived direct and indirect interlayer excitons in van der Waals heterostructures. Nano Lett. 17, 5229–5237. https://doi.org/10.1021/acs.nanolett.7b01304.

Mounet, N., Gibertini, M., Schwaller, P., Campi, D., Merkys, A., Marrazzo, A., Sohier, T., Castelli, I.E., Cepellotti, A., Pizzi, G., and Marzari, N. (2018). Two-dimensional materials from high-throughput computational exfoliation of experimentally known compounds. Nat. Nanotech 13, 246–252. https://doi.org/10.1038/s41565-017-0035-5.

Mukherjee, A., Shayan, K., Li, L., Shan, J., Mak, K.F., and Vamivakas, A.N. (2020). Observation of site-controlled localized charged excitons in CrI3/WSe2 heterostructures. Nat. Commun. 11, 5502. https://doi.org/10.1038/s41467-020-19262-2.

Nourbakhsh, A., Zubair, A., Dresselhaus, M.S., and Palacios, T. (2016). Transport properties of a MoS_2/WSe_2 heterojunction transistor and its potential for application. Nano Lett. 16, 1359–1366. https://doi.org/10.1021/acs.nanolett.5b04791.

Novoselov, K.S., Geim, A.K., Morozov, S.V., Jiang, D., Zhang, Y., Dubonos, S.V., Grigorieva, I.V., and Firsov, A.A. (2004). Electric field effect in atomically thin carbon films. Science 306, 666–669. https://doi.org/10.1126/science.1102896.

Nugera, F.A., Sahoo, P.K., Xin, Y., Ambardar, S., Voronine, D.V., Kim, U.J., Han, Y., Son, H., and Gutiérrez, H.R. (2021). Bandgap engineering in 2D lateral heterostructures of transition metal dichalcogenides via controlled alloying. Small n/a, 2106600. https://doi.org/10.1002/smll.202106600.

Ohta, T., Robinson, J.T., Feibelman, P.J., Bostwick, A., Rotenberg, E., and Beechem, T.E. (2012). Evidence for interlayer coupling and moiré periodic potentials in twisted bilayer graphene. Phys. Rev. Lett. 109, 186807. https://doi.org/10.1103/PhysRevLett.109.186807.

Oliva, N., Backman, J., Capua, L., Cavalieri, M., Luisier, M., and Ionescu, A.M. (2020). WSe_2/$SnSe_2$ vdW heterojunction Tunnel FET with subthermionic characteristic and MOSFET co-integrated on same WSe flake. Npj 2D Mater Appl 4, 5. https://doi.org/10.1038/s41699-020-0142-2.

Omambac, K.M., Hattab, H., Brand, C., Jnawali, G., N'Diaye, A.T., Coraux, J., van Gastel, R., Poelsema, B., Michely, T., Meyer zu Heringdorf, F.-J., and Hoegen, M.H. (2019). Temperature-controlled rotational epitaxy of graphene. Nano Lett. 19, 4594–4600. https://doi.org/10.1021/acs.nanolett.9b01565.

Pandey, H., Shaygan, M., Sawallich, S., Kataria, S., Wang, Z., Noculak, A., Otto, M., Nagel, M., Negra, R., Neumaier, D., and Lemme, M.C. (2018). All CVD boron nitride encapsulated graphene FETs with CMOS compatible metal edge contacts. IEEE Trans. Electron Devices 65, 4129–4134. https://doi.org/10.1109/TED.2018.2865382.

Pradhan, N.R., Rhodes, D., Feng, S., Xin, Y., Memaran, S., Moon, B.-H., Terrones, H., Terrones, M., and Balicas, L. (2014). Field-effect transistors based on few-layered α-MoTe$_2$. ACS Nano 8, 5911–5920. https://doi.org/10.1021/nn501013c.

Radisavljevic, B., Radenovic, A., Brivio, J., Giacometti, V., and Kis, A. (2011). Single-layer MoS_2 transistors. Nat. Nanotech 6, 147–150. https://doi.org/10.1038/nnano.2010.279.

Regan, E.C., Wang, D., Jin, C., Bakti Utama, M.I., Gao, B., Wei, X., Zhao, S., Zhao, W., Zhang, Z., Yumigeta, K., et al. (2020). Mott and generalized Wigner crystal states in WSe_2/WS_2 moiré superlattices. Nature 579, 359–363. https://doi.org/10.1038/s41586-020-2092-4.

Rivera, P., Schaibley, J.R., Jones, A.M., Ross, J.S., Wu, S., Aivazian, G., Klement, P., Seyler, K., Clark, G., Ghimire, N.J., et al. (2015). Observation of long-lived interlayer excitons in monolayer MoSe$_2$–WSe$_2$ heterostructures. Nat. Commun. 6, 6242. https://doi.org/10.1038/ncomms7242.

Robert, C., Amand, T., Cadiz, F., Lagarde, D., Courtade, E., Manca, M., Taniguchi, T., Watanabe, K., Urbaszek, B., and Marie, X. (2017). Fine structure and lifetime of dark excitons in transition metal dichalcogenide monolayers. Phys. Rev. B 96, 155423. https://doi.org/10.1103/PhysRevB.96.155423.

Roy, T., Tosun, M., Kang, J.S., Sachid, A.B., Desai, S.B., Hettick, M., Hu, C.C., and Javey, A. (2014). Field-effect transistors built from all two-dimensional material components. ACS Nano 8, 6259–6264. https://doi.org/10.1021/nn501723y.

Sahoo, P.K., Memaran, S., Nugera, F.A., Xin, Y., Díaz Márquez, T., Lu, Z., Zheng, W., Zhigadlo, N.D., Smirnov, D., Balicas, L., and Gutiérrez, H.R. (2019). Bilayer lateral heterostructures of transition-metal dichalcogenides and their optoelectronic response. ACS Nano 13, 12372–12384. https://doi.org/10.1021/acsnano.9b04957.

Sahoo, P.K., Memaran, S., Xin, Y., Balicas, L., and Gutiérrez, H.R. (2018). One-pot growth of two-dimensional lateral heterostructures via sequential edge-epitaxy. Nature 553, 63–67. https://doi.org/10.1038/nature25155.

Sangwan, V.K., Jariwala, D., Kim, I.S., Chen, K.-S., Marks, T.J., Lauhon, L.J., and Hersam, M.C. (2015). Gate-tunable memristive phenomena mediated by grain boundaries in single-layer MoS2. Nat. Nanotech 10, 403–406. https://doi.org/10.1038/nnano.2015.56.

Sangwan, V.K., Lee, H.-S., Bergeron, H., Balla, I., Beck, M.E., Chen, K.-S., and Hersam, M.C. (2018). Multi-terminal memtransistors from polycrystalline monolayer molybdenum disulfide. Nature 554, 500–504. https://doi.org/10.1038/nature25747.

Sarkar, D., Liu, W., Xie, X., Anselmo, A.C., Mitragotri, S., and Banerjee, K. (2014). MoS2 field-effect transistor for next-generation label-free biosensors. ACS Nano 8, 3992–4003. https://doi.org/10.1021/nn5009148.

Sarkar, D., Xie, X., Liu, W., Cao, W., Kang, J., Gong, Y., Kraemer, S., Ajayan, P.M., and Banerjee, K. (2015). A subthermionic tunnel field-effect transistor with an atomically thin channel. Nature 526, 91–95. https://doi.org/10.1038/nature15387.

Seyler, K.L., Rivera, P., Yu, H., Wilson, N.P., Ray, E.L., Mandrus, D.G., Yan, J., Yao, W., and Xu, X. (2019). Signatures of moiré-trapped valley excitons in MoSe$_2$/WSe$_2$ heterobilayers. Nature 567, 66–70. https://doi.org/10.1038/s41586-019-0957-1.

Seyler, K.L., Zhong, D., Huang, B., Linpeng, X., Wilson, N.P., Taniguchi, T., Watanabe, K., Yao, W., Xiao, D., McGuire, M.A., et al. (2018). Valley manipulation by optically tuning the magnetic proximity effect in WSe2/CrI3 heterostructures. Nano Lett. 18, 3823–3828. https://doi.org/10.1021/acs.nanolett.8b01105.

Shen, P.-C., Su, C., Lin, Y., Chou, A.-S., Cheng, C.-C., Park, J.-H., Chiu, M.-H., Lu, A.-Y., Tang, H.-L., Tavakoli, M.M., et al. (2021). Ultralow contact resistance between semimetal and monolayer semiconductors. Nature 593, 211–217. https://doi.org/10.1038/s41586-021-03472-9.

Soluyanov, A.A., Gresch, D., Wang, Z., Wu, Q., Troyer, M., Dai, X., and Bernevig, B.A. (2015). Type-II Weyl semimetals. Nature 527, 495–498. https://doi.org/10.1038/nature15768.

Song, H., Ni, Y., and Kokot, S. (2014). Investigations of an electrochemical platform based on the layered MoS2–graphene and horseradish peroxidase nanocomposite for direct electrochemistry and electrocatalysis. Biosens. Bioelectron. 56, 137–143. https://doi.org/10.1016/j.bios.2014.01.014.

Song, W.G., Kwon, H.-J., Park, J., Yeo, J., Kim, M., Park, S., Yun, S., Kyung, K.-U., Grigoropoulos, C.P., Kim, S., and Hong, Y.K. (2016). High-performance flexible multilayer MoS2 transistors on solution-based polyimide substrates. Adv. Funct. Mater. 26, 2426–2434. https://doi.org/10.1002/adfm.201505019.

Sousa, F.B., Lafeta, L., Cadore, A.R., Sahoo, P.K., and Malard, L.M. (2021). Revealing atomically sharp interfaces of two-dimensional lateral heterostructures by second harmonic generation. 2D Mater. 8, 035051. https://doi.org/10.1088/2053-1583/ac0731.

Srivastava, P.K., Hassan, Y., de Sousa, D.J.P., Gebredingle, Y., Joe, M., Ali, F., Zheng, Y., Yoo, W.J., Ghosh, S., Teherani, J.T., et al. (2021). Resonant tunnelling diodes based on twisted black phosphorus homostructures. Nat.Electron 4, 269–276. https://doi.org/10.1038/s41928-021-00549-1.

Sun, J., Lin, N., Tang, C., Ren, H., and Zhao, X. (2017). A first principles study of the interaction between two-dimensional black phosphorus and Al_2O_3 dielectric. RSC Adv. *7*, 13777–13783. https://doi.org/10.1039/C6RA27271A.

Sun, L., Wang, Z., Wang, Y., Zhao, L., Li, Y., Chen, B., Huang, S., Zhang, S., Wang, W., Pei, D., et al. (2021). Hetero-site nucleation for growing twisted bilayer graphene with a wide range of twist angles. Nat. Commun. *12*, 2391. https://doi.org/10.1038/s41467-021-22533-1.

Tang, Y., Li, L., Li, T., Xu, Y., Liu, S., Barmak, K., Watanabe, K., Taniguchi, T., MacDonald, A.H., Shan, J., and Mak, K.F. (2020). Simulation of Hubbard model physics in WSe 2/WS 2 moiré superlattices. Nature *579*, 353–358. https://doi.org/10.1038/s41586-020-2085-3.

Tang, Y., Mak, K.F., and Shan, J. (2019). Long valley lifetime of dark excitons in single-layer WSe 2. Nat. Commun. *10*, 4047. https://doi.org/10.1038/s41467-019-12129-1.

Tran, K., Moody, G., Wu, F., Lu, X., Choi, J., Kim, K., Rai, A., Sanchez, D.A., Quan, J., Singh, A., et al. (2019). Evidence for moiré excitons in van der Waals heterostructures. Nature *567*, 71–75. https://doi.org/10.1038/s41586-019-0975-z.

Trushin, M., Sarkar, S., Mathew, S., Goswami, S., Sahoo, P., Wang, Y., Yang, J., Li, W., MacManus-Driscoll, J.L., Chhowalla, M., et al. (2020). Evidence of rotational Fröhlich coupling in polaronic trions. Phys. Rev. Lett. *125*, 086803. https://doi.org/10.1103/PhysRevLett.125.086803.

Unuchek, D., Ciarrocchi, A., Avsar, A., Sun, Z., Watanabe, K., Taniguchi, T., and Kis, A. (2019). Valley-polarized exciton currents in a van der Waals heterostructure. Nat. Nanotechnol. *14*, 1104–1109. https://doi.org/10.1038/s41565-019-0559-y.

Unuchek, D., Ciarrocchi, A., Avsar, A., Watanabe, K., Taniguchi, T., and Kis, A. (2018). Room-temperature electrical control of exciton flux in a van der Waals heterostructure. Nature *560*, 340–344. https://doi.org/10.1038/s41586-018-0357-y.

Vizner Stern, M., Waschitz, Y., Cao, W., Nevo, I., Watanabe, K., Taniguchi, T., Sela, E., Urbakh, M., Hod, O., and Ben Shalom, M. (2021). Interfacial ferroelectricity by van der Waals sliding. Science *372*, 1462–1466. https://doi.org/10.1126/science.abe8177.

Wang, E., Lu, X., Ding, S., Yao, W., Yan, M., Wan, G., Deng, K., Wang, S., Chen, G., Ma, L., et al. (2016). Gaps induced by inversion symmetry breaking and second-generation Dirac cones in graphene/hexagonal boron nitride. Nat. Phys *12*, 1111–1115. https://doi.org/10.1038/nphys3856.

Wang, J., Rousseau, A., Yang, M., Low, T., Francoeur, S., and Kéna-Cohen, S. (2020). Mid-infrared polarized emission from black phosphorus light-emitting diodes. Nano Lett. *20*, 3651–3655. https://doi.org/10.1021/acs.nanolett.0c00581.

Wang, S., Crowther, J., Kageshima, H., Hibino, H., and Taniyasu, Y. (2021a). Epitaxial intercalation growth of scalable hexagonal boron nitride/graphene bilayer moiré materials with highly convergent interlayer angles. ACS Nano *15*,

14384–14393. https://doi.org/10.1021/acsnano.1c03698.

Wang, S., Cui, X., Jian, C., Cheng, H., Niu, M., Yu, J., Yan, J., and Huang, W. (2021b). Stacking-engineered heterostructures in transition metal dichalcogenides. Adv. Mater. *33*, 2005735. https://doi.org/10.1002/adma.202005735.

Wang, X., Gong, Y., Shi, G., Chow, W.L., Keyshar, K., Ye, G., Vajtai, R., Lou, J., Liu, Z., Ringe, E., et al. (2014). Chemical vapor deposition growth of crystalline monolayer MoSe 2. ACS Nano *8*, 5125–5131. https://doi.org/10.1021/nn501175k.

Wang, X., Yu, P., Lei, Z., Zhu, C., Cao, X., Liu, F., You, L., Zeng, Q., Deng, Y., Zhu, C., et al. (2019a). Van der Waals negative capacitance transistors. Nat. Commun. *10*, 3037. https://doi.org/10.1038/s41467-019-10738-4.

Wang, Y., Kim, J.C., Wu, R.J., Martinez, J., Song, X., Yang, J., Zhao, F., Mkhoyan, A., Jeong, H.Y., and Chhowalla, M. (2019b). Van der Waals contacts between three-dimensional metals and two-dimensional semiconductors. Nature *568*, 70–74. https://doi.org/10.1038/s41586-019-1052-3.

Wang, Z., Rhodes, D.A., Watanabe, K., Taniguchi, T., Hone, J.C., Shan, J., and Mak, K.F. (2019c). Evidence of high-temperature exciton condensation in two-dimensional atomic double layers. Nature *574*, 76–80. https://doi.org/10.1038/s41586-019-1591-7.

Wang, Z., Xie, Y., Wang, H., Wu, R., Nan, T., Zhan, Y., Sun, J., Jiang, T., Zhao, Y., Lei, Y., et al. (2017). NaCl-assisted one-step growth of MoS2–WS2in-plane heterostructures. Nanotechnology *28*, 325602. https://doi.org/10.1088/1361-6528/aa6f01.

Wu, E., Xie, Y., Wang, S., Zhang, D., Hu, X., and Liu, J. (2020). Non-volatile programmable homogeneous lateral MoTe2 junction for multi-bit flash memory and high-performance optoelectronics. Nano Res. *13*, 3445–3451. https://doi.org/10.1007/s12274-020-3041-0.

Wu, F., Lovorn, T., and MacDonald, A.H. (2018a). Theory of optical absorption by interlayer excitons in transition metal dichalcogenide heterobilayers. Phys. Rev. B *97*, 035306. https://doi.org/10.1103/PhysRevB.97.035306.

Wu, F., Xia, H., Sun, H., Zhang, J., Gong, F., Wang, Z., Chen, L., Wang, P., Long, M., Wu, X., et al. (2019a). AsP/InSe van der Waals tunneling heterojunctions with ultrahigh reverse rectification ratio and high photosensitivity. Adv. Funct. Mater. *29*, 1900314. https://doi.org/10.1002/adfm.201900314.

Wu, P., Ameen, T., Zhang, H., Bendersky, L.A., Ilatikhameneh, H., Klimeck, G., Rahman, R., Davydov, A.V., and Appenzeller, J. (2019b). Complementary black phosphorus tunneling field-effect transistors. ACS Nano *13*, 377–385. https://doi.org/10.1021/acsnano.8b06441.

Wu, R., Tao, Q., Dang, W., Liu, Y., Li, B., Li, J., Zhao, B., Zhang, Z., Ma, H., Sun, G., et al. (2019c). van der Waals epitaxial growth of atomically thin 2D metals on dangling-bond-free WSe2 and WS2. Adv. Funct. Mater. *29*, 1806611. https://doi.org/10.1002/adfm.201806611.

Wu, S., Fatemi, V., Gibson, Q.D., Watanabe, K., Taniguchi, T., Cava, R.J., and Jarillo-Herrero, P. (2018b). Observation of the quantum spin Hall effect up to 100 kelvin in a monolayer crystal. Science *359*, 76–79.

Xia, Q., and Yang, J.J. (2019). Memristive crossbar arrays for brain-inspired computing. Nat. Mater. *18*, 309–323. https://doi.org/10.1038/s41563-019-0291-x.

Xiang, D., Liu, T., Xu, J., Tan, J.Y., Hu, Z., Lei, B., Zheng, Y., Wu, J., Neto, A.H.C., Liu, L., and Chen, W. (2018). Two-dimensional multibit optoelectronic memory with broadband spectrum distinction. Nat. Commun. *9*, 2966. https://doi.org/10.1038/s41467-018-05397-w.

Xiao, D., Liu, G.-B., Feng, W., Xu, X., and Yao, W. (2012). Coupled spin and valley physics in monolayers of MoS_2 and other group-VI dichalcogenides. Phys. Rev. Lett. *108*, 196802. https://doi.org/10.1103/PhysRevLett.108.196802.

Xie, S., Tu, L., Han, Y., Huang, L., Kang, K., Lao, K.U., Poddar, P., Park, C., Muller, D.A., DiStasio, R.A., and Park, J. (2018). Coherent, atomically thin transition-metal dichalcogenide superlattices with engineered strain. Science *359*, 1131–1136. https://doi.org/10.1126/science.aao5360.

Xu, L., Wang, Y., Hsiao, C., Ni, I., Chen, M., and Wu, C. (2021). Enhanced electrical performance of van der Waals heterostructure. Adv. Mater. Inter. *8*, 2001850. https://doi.org/10.1002/admi.202001850.

Yan, R., Fathipour, S., Han, Y., Song, B., Xiao, S., Li, M., Ma, N., Protasenko, V., Muller, D.A., Jena, D., and Xing, H.G. (2015). Esaki diodes in van der Waals heterojunctions with broken-gap energy band Alignment. Nano Lett. *15*, 5791–5798. https://doi.org/10.1021/acs.nanolett.5b01792.

Yan, W., Txoperena, O., Llopis, R., Dery, H., Hueso, L.E., and Casanova, F. (2016). A two-dimensional spin field-effect switch. Nat. Commun. *7*, 13372. https://doi.org/10.1038/ncomms13372.

Yan, X., Liu, C., Li, C., Bao, W., Ding, S., Zhang, D.W., and Zhou, P. (2017). Tunable SnSe 2/WSe 2 heterostructure tunneling field effect transistor. Small *13*, 1701478. https://doi.org/10.1002/smll.201701478.

Yang, C.-W., Tang, H.-L., Sattar, S., Chiu, M.-H., Wan, Y., Chen, C.-H., Kong, J., Huang, K.-W., Li, L.-J., and Tung, V. (2020). Epitaxial growth and determination of band Alignment of Bi2Te3–WSe2 vertical van der Waals heterojunctions. ACS Mater. Lett *2*, 1351–1359. https://doi.org/10.1021/acsmaterialslett.0c00254.

Yang, T., Zheng, B., Wang, Z., Xu, T., Pan, C., Zou, J., Zhang, X., Qi, Z., Liu, H., Feng, Y., et al. (2017). Van der Waals epitaxial growth and optoelectronics of large-scale WSe2/SnS2 vertical bilayer p–n junctions. Nat. Commun. *8*, 1906. https://doi.org/10.1038/s41467-017-02093-z.

Yankowitz, M., Xue, J., Cormode, D., Sanchez-Yamagishi, J.D., Watanabe, K., Taniguchi, T., Jarillo-Herrero, P., Jacquod, P., and LeRoy, B.J. (2012). Emergence of superlattice Dirac points in graphene on hexagonal boron nitride. Nat. Phys *8*, 382–386. https://doi.org/10.1038/nphys2272.

Yasuda, K., Wang, X., Watanabe, K., Taniguchi, T., and Jarillo-Herrero, P. (2021). Stacking-engineered ferroelectricity in bilayer boron nitride. Science *372*, 1458–1462. https://doi.org/10.1126/science.abd3230.

Yoon, J., Park, W., Bae, G.-Y., Kim, Y., Jang, H.S., Hyun, Y., Lim, S.K., Kahng, Y.H., Hong, W.-K., Lee, B.H., and Ko, H.C. (2013). Highly flexible and transparent multilayer MoS $_2$ transistors with graphene electrodes. Small n/a-n/a *9*, 3295–3300. https://doi.org/10.1002/smll.201300134.

Yuan, L., Zheng, B., Kunstmann, J., Brumme, T., Kuc, A.B., Ma, C., Deng, S., Blach, D., Pan, A., and Huang, L. (2020). Twist-angle-dependent interlayer exciton diffusion in WS $_2$ –WSe $_2$ heterobilayers. Nat. Mater. *19*, 617–623. https://doi.org/10.1038/s41563-020-0670-3.

Zeng, H., Dai, J., Yao, W., Xiao, D., and Cui, X. (2012). Valley polarization in MoS $_2$ monolayers by optical pumping. Nat. Nanotech *7*, 490–493. https://doi.org/10.1038/nnano.2012.95.

Zhai, X., Xu, X., Peng, J., Jing, F., Zhang, Q., Liu, H., and Hu, Z. (2020). Enhanced optoelectronic performance of CVD-grown metal–semiconductor NiTe2/MoS2 heterostructures. ACS Appl. Mater. Inter. *12*, 24093–24101. https://doi.org/10.1021/acsami.0c02166.

Zhang, C., Chuu, C.-P., Ren, X., Li, M.-Y., Li, L.-J., Jin, C., Chou, M.-Y., and Shih, C.-K. (2017a). Interlayer couplings, Moiré patterns, and 2D electronic superlattices in MoS2/WSe $_2$ heterobilayers. Sci. Adv. *3*, e1601459. https://doi.org/10.1126/sciadv.1601459.

Zhang, X., Grajal, J., Vazquez-Roy, J.L., Radhakrishna, U., Wang, X., Chern, W., Zhou, L., Lin, Y., Shen, P.-C., Ji, X., et al. (2019a). Two-dimensional MoS2-enabled flexible rectenna for Wi-Fi-band wireless energy harvesting. Nature *566*, 368–372. https://doi.org/10.1038/s41586-019-0892-1.

Zhang, X., Xiao, S., Nan, H., Mo, H., Wan, X., Gu, X., and Ostrikov, K. (2018). Controllable one-step growth of bilayer MoS2–WS2/WS2 heterostructures by chemical vapor deposition. Nanotechnology *29*, 455707. https://doi.org/10.1088/1361-6528/aaddc5.

Zhang, X.-Q., Lin, C.-H., Tseng, Y.-W., Huang, K.-H., and Lee, Y.-H. (2015). Synthesis of lateral heterostructures of semiconducting atomic layers. Nano Lett. *15*, 410–415. https://doi.org/10.1021/nl503744f.

Zhang, Z., Chen, P., Duan, X., Zang, K., Luo, J., and Duan, X. (2017b). Robust epitaxial growth of two-dimensional heterostructures, multiheterostructures, and superlattices. Science *357*, 788–792. https://doi.org/10.1126/science.aan6814.

Zhang, Z., Gong, Y., Zou, X., Liu, P., Yang, P., Shi, J., Zhao, L., Zhang, Q., Gu, L., and Zhang, Y. (2019b). Epitaxial growth of two-dimensional metal–semiconductor transition-metal dichalcogenide vertical stacks (VSe2/MX2) and their band Alignments. ACS Nano *13*, 885–893. https://doi.org/10.1021/acsnano.8b08677.

Zhao, B., Karpiak, B., Khokhriakov, D., Johansson, A., Hoque, A.M., Xu, X., Jiang, Y., Mertig, I., and Dash, S.P. (2020). Unconventional charge–spin conversion in weyl-semimetal WTe2. Adv. Mater. *32*, 2000818. https://doi.org/10.1002/adma.202000818.

Zhao, B., Ngaloy, R., Hoque, A.M., Karpiak, B., Khokhriakov, D., and Dash, S.P. (2021). Van der Waals magnet based spin-valve devices at room temperature. https://arxiv.org/abs/2107.00310.

Zhao, Y., and Jin, S. (2020). Controllable water vapor assisted chemical vapor transport synthesis of WS2–MoS $_2$ heterostructure. ACS Mater. Lett *2*, 42–48. https://doi.org/10.1021/acsmaterialslett.9b00415.

Zheng, Z., Ma, Q., Bi, Z., de la Barrera, S., Liu, M.-H., Mao, N., Zhang, Y., Kiper, N., Watanabe, K., Taniguchi, T., et al. (2020). Unconventional ferroelectricity in moiré heterostructures. Nature *588*, 71–76. https://doi.org/10.1038/s41586-020-2970-9.

Zhong, D., Seyler, K.L., Linpeng, X., Cheng, R., Sivadas, N., Huang, B., Schmidgall, E., Taniguchi, T., Watanabe, K., McGuire, M.A., et al. (2017). Van der Waals engineering of ferromagnetic semiconductor heterostructures for spin and valleytronics. Sci. Adv. *3*, e1603113. https://doi.org/10.1126/sciadv.1603113.

Zhong, D., Seyler, K.L., Linpeng, X., Wilson, N.P., Taniguchi, T., Watanabe, K., McGuire, M.A., Fu, K.-M.C., Xiao, D., Yao, W., and Xu, X. (2020). Layer-resolved magnetic proximity effect in van der Waals heterostructures. Nat. Nanotechnol. *15*, 187–191. https://doi.org/10.1038/s41565-019-0629-1.

Zhou, W., Zhang, Y.-Y., Chen, J., Li, D., Zhou, J., Liu, Z., Chisholm, M.F., Pantelides, S.T., and Loh, K.P. (2018). Dislocation-driven growth of two-dimensional lateral quantum-well superlattices. Sci. Adv. *4*, eaap9096. https://doi.org/10.1126/sciadv.aap9096.

Zhou, Y., Scuri, G., Wild, D.S., High, A.A., Dibos, A., Jauregui, L.A., Shu, C., De Greve, K., Pistunova, K., Joe, A.Y., et al. (2017). Probing dark excitons in atomically thin semiconductors via near-field coupling to surface plasmon polaritons. Nat. Nanotech *12*, 856–860. https://doi.org/10.1038/nnano.2017.106.

Zhu, C., Sun, X., Liu, H., Zheng, B., Wang, X., Liu, Y., Zubair, M., Wang, X., Zhu, X., Li, D., and Pan, A. (2019). Nonvolatile MoTe2 p–n diodes for optoelectronic logics. ACS Nano *13*, 7216–7222. https://doi.org/10.1021/acsnano.9b02817.

Zhu, J., Li, W., Huang, R., Ma, L., Sun, H., Choi, J.-H., Zhang, L., Cui, Y., and Zou, G. (2020). One-pot selective epitaxial growth of large WS2/MoS2 lateral and vertical heterostructures. J. Am. Chem. Soc. *142*, 16276–16284. https://doi.org/10.1021/jacs.0c05691.

Zhu, K., Wen, C., Aljarb, A.A., Xue, F., Xu, X., Tung, V., Zhang, X., Alshareef, H.N., and Lanza, M. (2021). The development of integrated circuits based on two-dimensional materials. Nat.Electron *4*, 775–785. https://doi.org/10.1038/s41928-021-00672-z.

Zollner, K., Gmitra, M., and Fabian, J. (2020). Swapping exchange and spin-orbit coupling in 2D van der Waals heterostructures. Phys. Rev. Lett. *125*, 196402. https://doi.org/10.1103/PhysRevLett.125.196402.

Zomer, P.J., Dash, S.P., Tombros, N., and van Wees, B.J. (2011). A transfer technique for high mobility graphene devices on commercially available hexagonal boron nitride. Appl. Phys. Lett. *99*, 232104. https://doi.org/10.1063/1.3665405.

Zomer, P.J., Guimarães, M.H.D., Brant, J.C., Tombros, N., and van Wees, B.J. (2014). Fast pick up technique for high quality heterostructures of bilayer graphene and hexagonal boron nitride. Appl. Phys. Lett. *105*, 013101. https://doi.org/10.1063/1.4886096.

Zou, Z., Liang, J., Zhang, X., Ma, C., Xu, P., Yang, X., Zeng, Z., Sun, X., Zhu, C., Liang, D., et al. (2021). Liquid-metal-assisted growth of vertical GaSe/MoS2 p–n heterojunctions for sensitive self-driven photodetectors. ACS Nano *15*, 10039–10047. https://doi.org/10.1021/acsnano.1c01643.